Earth's Future

RESEARCH ARTICLE

10.1029/2025EF007594

Disaggregation of Landslide Risk

William Pollock[1] and Joseph Wartman[1]

[1]Department of Civil and Environmental Engineering, University of Washington, Seattle, WA, USA

Key Points:

- A transferable probabilistic landslide risk analysis model quantifies building-level landslide risk—a critical capability absent from traditional susceptibility maps
- Risk disaggregation reveals that dominant landslide hazards and triggers can vary dramatically between neighboring properties
- Current susceptibility-based policies can be dangerously incomplete; landslide runout is a primary, yet often overlooked, driver of risk

Supporting Information:

Supporting Information may be found in the online version of this article.

Correspondence to:

W. Pollock,
wpollock14@gmail.com

Citation:

Pollock, W., & Wartman, J. (2026). Disaggregation of landslide risk. *Earth's Future*, *14*, e2025EF007594. https://doi.org/10.1029/2025EF007594

Received 30 OCT 2025
Accepted 6 MAR 2026

Abstract

Quantifying and disaggregating landslide risk through probabilistic landslide risk analysis (PLRA) is critical for land use regulation and risk reduction. However, no transferable model for PLRA currently exists that resolves landslide consequences to individual buildings at regional scales. We introduce the physically-based MM_3 model for multimodal landslide risk analysis and apply it to Seattle, Washington, USA. Frequent precipitation-induced shallow landslides govern landslide risk in Seattle, although ground shaking from infrequent earthquakes, such as those anticipated on the Seattle Fault and Cascadia Subduction Zone, could expose over 60,000 people and 12,000 buildings to landslides. Critically, building-specific risk profiles vary by orders-of-magnitude even at neighboring properties, with different landslide modes and triggers posing distinct threats to human life versus structural integrity—enabling highly tailored mitigation strategies. Significantly more buildings face landslide risk than are currently designated as landslide-prone under susceptibility-based policies, primarily due to runout being excluded in susceptibility mapping. By quantifying and disaggregating landslide risk at building resolution across regional scales, MM_3 provides a foundation for translating landslide science into actionable, risk-informed land use policy.

Plain Language Summary

Landslides are a damaging and deadly hazard globally. However, current approaches to managing landslides rely primarily on susceptibility maps that show where landslides *might* occur, without quantifying *how often* failures happen and *how far* debris might travel (i.e., landslide hazard), or *what damage* could result (i.e., landslide risk). This makes it difficult for communities to decide where development is safe. In this study, we introduce a new framework that estimates building-level landslide risk across entire cities and regions, expressing risk in terms that people can easily understand and compare: financial losses and threats to life. Applying our model to the landslide-prone city of Seattle, Washington, USA, we find that landslides triggered by frequent rain cause more damage over time than those from catastrophic but infrequent earthquakes. Risk varies dramatically over short distances—even between adjacent properties—and, counterintuitively, where landslides most frequently occur is not necessarily where they cause the most harm. Different landslide types and triggers pose unique threats to humans versus structures, enabling tailored risk reduction strategies. This framework represents a critical step toward making landslide risk assessment practical and accessible for cities and regions worldwide that face increasing landslide threats from climate change and urban expansion.

1. Introduction

Landslides pose significant threats to lives and infrastructure worldwide. These threats heighten as human populations expand into hazard-prone terrain, and climate change and land use intensification alter environmental systems (IPCC, 2022; UNDRR, 2022). As a result, human exposure to landslide hazards is increasing in both frequency and intensity (Froude & Petley, 2018), amplifying risk and challenging societal resilience. Effective risk reduction and sustainable land management in this changing world require robust, quantitative knowledge of hazard and risk (Crozier & Glade, 2005; UNDRR, 2017).

However, current land use planning and policy approaches are predominantly based on landslide susceptibility mapping (Reichenbach et al., 2018; van Westen et al., 2006). Susceptibility maps indicate only spatial zones of relative likelihood of failure; they typically lack essential information about the type, size, mobility, and timing (i.e., *landslide hazard*), or consequences (i.e., *landslide risk*) of potential landslides (Hungr et al., 2016; Mirus et al., 2024). This fundamental disconnect between susceptibility mapping and quantitative risk estimation hinders effective decision-making and has contributed to catastrophic outcomes, including the deadly 2018 Montecito, California, and 2014 Oso, Washington, landslides (Lancaster et al., 2021; Wartman et al., 2016). This is especially important because the relationship between landslide susceptibility and societal risk is often nonlinear; areas of highest susceptibility do not always correspond to areas of highest risk, which is a function of

10.1029/2025EF007594

the specific population and infrastructure exposed. Transitioning from susceptibility-based to risk-informed land use planning is therefore crucial for building resilient communities in the face of future environmental change.

Probabilistic Landslide Risk Analysis (PLRA) offers a rigorous, quantitative framework to address this gap. PLRA integrates multiple credible scenarios—considering different modes, magnitudes, and triggering events—to estimate the annualized potential for loss at specific locations. Similar to Probabilistic Seismic Hazard Analysis (PSHA), the widely adopted standard for earthquake hazards (Cornell, 1968), PLRA provides decision makers with an objective, reproducible, and comparable metric. This enables them to evaluate risks, assess mitigation benefits, and transparently communicate complex hazards (de Vilder et al., 2022; Strouth & McDougall, 2022). Furthermore, PLRA enables the disaggregation of total landslide risk into its component sources, as PSHA does for earthquake hazard (Bazzurro & Cornell, 1999). Landslide risk disaggregation provides critical insights for targeted risk reduction strategies. Despite these advantages for informing resilient development, PLRA is rarely applied comprehensively at the regional scales relevant for land use planning largely due to the lack of a practical, transferable modeling framework and the difficulty of integrating disparate and scarce data sets (Dixon et al., 2023; Izenberg et al., 2022; Van Westen et al., 2006).

Addressing these challenges, this study introduces a novel, portable framework for regional-scale PLRA that is designed to overcome limitations in existing susceptibility-based approaches and provide a quantitative basis for land use decisions and building resilience. This framework integrates multiple triggering mechanisms (precipitation and seismic shaking) and distinct failure modes—a critical feature, as different landslide types have vastly different consequences for human occupants versus the structures themselves. Unlike most susceptibility mapping, it includes explicit runout modeling to determine impact zones. Crucially, the model's ability to disaggregate risk reveals the specific drivers—such as failure mode or trigger type—at any given location, creating detailed risk profiles that can inform tailored mitigation strategies. This high-resolution approach also provides a direct, quantitative means to evaluate the efficacy of current susceptibility-based land use policies.

To demonstrate the implementation and utility of this framework, we selected Seattle, Washington, as an exemplar case study. Seattle provides a robust testing ground for a comprehensive PLRA model due to several factors: (a) it is a dense urban environment with significant elements at risk; (b) it possesses a complex, multi-hazard landscape with both precipitation- and earthquake-induced landslide triggers; (c) its well-documented glacial geology generates diverse failure modes; and (d) the availability of high-quality historical landslide and geotechnical data allows for robust model tailoring and first-order validation. By demonstrating the framework in this setting, we establish a methodology that can be adapted for other complex environments globally.

Importantly, this application allows quantitative exploration of key questions for risk-based land use policy, including:

- To what extent do different landslide modes (e.g., shallow slides vs. deep-seated slumps) and triggers (precipitation vs. seismic) control the risk profile at specific locations?
- How does the spatial distribution of landslide risk intersect with patterns of urban development, and what are the implications for hazard exposure across different parts of a community?
- How do traditional susceptibility-based land use planning approaches compare to quantitative risk assessments in characterizing the true potential danger from landslides?
- How can granular, building-level risk profiles be used to develop more effective, tailored, and data-driven land use policies and community resilience strategies?

Using our framework, we find that total landslide risk and the relative contributions of different landslide types can vary by orders of magnitude between neighboring locations, highlighting the limitations of existing statutory susceptibility maps. By providing both spatially distributed risk metrics and the ability to disaggregate risk by landslide mode and consequence, this transferable methodology offers a pathway for developing more effective, targeted, and risk-informed land use policy in hazardous landscapes.

1.1. Quantitative Landslide Risk Analysis

Landslide risk analysis estimates landslide consequences across space and time for exposed elements within an area of interest. In is generalized form, quantitative risk is the summation of a series of probabilities describing independent landslide events and the element(s) of interest which they impact:

$$R_{j\,(\text{Loss of Life})} = \sum_1^n h_i \; x \; S_{i,j} \; x \; T_{i,j} \; x \;\; V_{i,j} \; x \; E \tag{1}$$

where R_j is the annual probability of death of individual j or the annual damage to building j; h_i is the annual probability of landslide scenario i occurring out of n total scenarios (*initiation hazard*); $S_{i,j}$ is the spatial probability of landslide i reaching a location commonly occupied by the element at risk, j (*runout*); $T_{i,j}$ is the spatial-temporal probability of the element at risk being in the location affected by the landslide at the time of occurrence (*exposure*); $V_{i,j}$ is the probability of death or degree of damage if the element at risk is present and impacted by the landslide (*vulnerability*); and E is the resident population or monetary value for infrastructural elements at risk (Fell et al., 2005; Lee & Jones, 2023; Strouth & McDougall, 2022; van Westen et al., 2006). Total landslide risk combines the specific risk for all possible types and magnitudes of landslides potentially impacting each element at risk.

1.2. Multimodal Model

We use the third generation of the multimodal model for landslide hazard analysis (Pollock & Wartman, 2025), herein referred to as "MM_3," which updates and expands the first ("MM_1") and second ("MM_2") generations introduced by Grant et al. (2016) and Pollock et al. (2019), respectively. The multimodal model analyzes the unique hazard and risk of different landslides modes through an integrated suite of mode-specific computational "modules" representing different components of the generalized risk equation (Equation 1). Key updates in MM_3 include groundwater modeling, explicit runout modeling, and flexible vulnerability modules, and implementation in a probabilistic (Monte Carlo), rather than deterministic framework.

MM_3 estimates landslide risk through the following steps:

1. Grid-based Factor of Safety (FS) is estimated using mode-specific physics-based models and remotely-sensed data, geologic mapping, and triggering scenarios (precipitation, seismic shaking).
2. Adjacent unstable terrain pixels are aggregated into landslide source zones, and the associated volume is estimated from the pre-defined failure geometry in Step (1).
3. Runout from each source zone is predicted using a statistical-empirical runout model.
4. Vulnerability is estimated from mode-specific empirical relationships, based on the landslide intensity (e.g., volume, depth, kinetic energy) and attributes of the elements at risk.
5. Risk is calculated, per Equation 1, for each element at risk, from each landslide mode and triggering scenario.

The methodology and generalized, location-agnostic version of MM_3 are detailed in Pollock and Wartman (2025). In this study, we present its application, tailoring the generalized model to a complex, multihazard urban environment where high-quality geohazard data allowed for robust assessment, as described in the following sections.

2. Application to Seattle, Washington, USA

2.1. Natural Environment of Seattle

2.1.1. Topography and Geology

Seattle occupies a ∼230 km^2 hourglass-shaped isthmus bordered by the glacial troughs of the Puget Sound and Lake Washington. Seattle's topography is characterized by glacially sculpted north-south ridges and steep coastal bluffs dissected by cross-cutting Quaternary drainages (Troost & Booth, 2008). Subsurface conditions reflect this glacial history. Glacial deposits from the Vashon Stade of the Fraser Glaciation (∼16 ka) predominate in the near surface, with a characteristic top-down stratigraphic sequence including loose recessional outwash, heavily overconsolidated lodgement till, advance outwash sand, and glaciolacustrine clay overlying very dense sand, silt, and gravel beds from the Olympia Interglaciation (Troost & Booth, 2008; Figure S1 in Supporting Information S1). Bedrock is exposed only locally in southeastern Seattle.

Most landslides occur at the contact between the advance outwash and glaciolacustrine clay where this contact is exposed along Seattle's steep coastal bluffs and inland ridges (Tubbs, 1974). Surface runoff infiltrates through the coarse-grained outwash and then is diverted laterally along the contact with the fine-grained material below. Episodic shallow (<3 m deep) debris flows and avalanches in saturated outwash mobilize material along the top

10.1029/2025EF007594

of the glaciolacustrine clay, creating a benched topography blanketed in loose, mobile colluvium. These shallow failures undercut the more competent till cap, which can subsequently fail in block falls and avalanches similar to an argillaceous rock (Laprade & Tubbs, 2008; Shipman, 2001). In contrast, deep-seated (>3 m deep) rotational slumps often involve both the coarse- and fine-grained units (Gerstel et al., 1997).

The City of Seattle Landslide Inventory catalogs 2,100 landslides from 1897 to 2019 (Davis et al., 2022; Seattle GeoData, 2023; Figure S2 in Supporting Information S1). The Landslide Inventory underpins most landslide studies in Seattle (Laprade et al., 2000; see Table S2 in Supporting Information S1), as well as the City's "landslide-prone" (susceptible) zone mapping and associated land use policies. However, these zones do not consider the timing, runout, or potential damage from landslides (Seattle OEM, 2019). Coe et al. (2000, 2004) developed the first comprehensive maps of quantitative, precipitation-induced landslide hazard for Seattle in the form of annual exceedance probabilities. Baum, Godt, and Highland (2008) and Baum, Savage, and Godt (2008) overviewed the state of the art in physically-based landslide hazard modeling for both deep and shallow landslides. Chleborad et al. (2008) developed rainfall intensity-duration thresholds that underpin Seattle's current real-time landslide occurrence forecasting (USGS, 2018). To date, no study has quantitatively analyzed landslide risk in Seattle. Given the physical basis of MM_3, we estimate landslide probability from the modeled magnitude-frequency curves of landslide triggering conditions (e.g., seismic shaking, rainfall) rather than from the Seattle Landslide Inventory, and we use the inventory as an independent, first-order validation of modeled hazard.

2.1.2. Seismicity and Climate

The Seattle area has three primary sources of seismic hazard: deep Benioff earthquakes within the subducting Juan de Fuca plate; shallow, crustal earthquakes within the North American plate, including on the Seattle Fault which crosscuts southern Seattle; and offshore, megathrust earthquakes in the Cascadia Subduction Zone. Deep earthquakes are the most frequent of these sources in Puget Sound, including the 1965 M6.7 Seattle-Tacoma earthquake and the 2001 M6.8 Nisqually earthquake (Chleborad & Schuster, 1990; Highland, 2003). Shallow crustal earthquakes are less frequent but potentially more damaging locally. The last major earthquake on the Seattle Fault was an M7.5 event ~1,100 years ago (Troost & Booth, 2008). Greater than M8.0 earthquakes on the Cascadia Subduction Zone have an estimated return period of 250–350 years (Grant, 2017), with the most recent event occurring in 1700 (Atwater et al., 2005).

Western Washington has a temperate maritime climate characterized by wet winters and relatively dry summers. Seattle receives ~950 mm of precipitation annually, three-quarters of which occurs from November to April (Godt et al., 2006; Neiman et al., 2011). Notably, moisture-laden atmospheric rivers from the tropics and subtropics are responsible for most of Western Washington's extreme precipitation events, such as a storm in October 2003 that dropped 128 mm of rain on Seattle in 24 hr (Neiman et al., 2011).

2.2. Model Inputs

The generalized version of MM_3 utilizes broadly available remotely-sensed data, facilitating baseline, standardized risk estimates globally (Pollock & Wartman, 2025). MM_3 can also accept local, higher-resolution data sets, where available. The following sections describe the local input data sets we used due to the high quality of geohazard information in Seattle.

2.2.1. Colluvium Depth

Colluvium mantles most hills in Seattle, ranging from centimeters to several meters above relatively unweathered glacial substrate. Many shallow landslides occur along this contact (Godt, Schultz, et al., 2008). Numerous physically-based and empirical colluvial depth models have been proposed, but most approaches are computationally expensive, overparameterized, or require extensive local calibration with field data (Lanni et al., 2012; Patton et al., 2018; Tefsa et al., 2009). MM_3 natively implements the data-parsimonious, curvature-based model of Patton et al. (2018); however, alternative models can be used depending on local soil formation and transport regime and data availability. Multiple colluvial depth models have been proposed for the Seattle area's glacially-sculpted hillslopes (Baum et al., 2010; Godt, Baum, et al., 2008; Godt, Schultz, et al., 2008; Schulz et al., 2008). We adopt the slope-based relationship of Godt, Baum, et al. (2008) due to its reproducibility, use of remotely sensed inputs, and consistency with observed shallow landslide depths in Seattle:

$$h = 7.72e^{(-0.04\beta)} \quad (2)$$

where β is the topographic slope in degrees. Colluvium depth predicted by Equation 2 ranges from a maximum of 7.72 m in flat locations to about 0.5 m on 68° slopes.

2.2.2. Material Parameters

Seattle's colluvial mantle necessitates defining two sets of material parameters within each geologic unit (Harp et al., 2006): that of the colluvium for shallow landslides and that of the underlying material for deep-seated rotational failures and rock/debris falls. We sampled material parameter values for Monte Carlo-based groundwater and stability modeling from distributions supported by previous geotechnical studies in Seattle. Text S2 and Tables S3–S4 in Supporting Information S1 provide the unit-specific parameter distributions and associated sources.

2.2.3. Root Cohesion

We calculated the normalized difference vegetation index (NDVI) from 3-m satellite imagery captured on 2 June 2019 (Planet Team, 2020). We defined ranges of NDVI associated with unvegetated surfaces, low vegetation, and dense tree cover. In moderately and densely vegetated areas (NDVI 0.35–0.63 and >0.63) we assigned root cohesion of 3 and 5 kPa, respectively, based on shrubs and trees common in the Pacific Northwest (Figure 1; Cislaghi et al., 2017; Schmidt et al., 2001).

2.2.4. Water Table Depth

We estimated the average wet- and dry-season groundwater table from 630 boring logs from the Washington Department of Natural Resources (DNR) Subsurface Database (Jeschke et al., 2016). We separated logs by date into wet season (November-April) and dry season (May-October). We related the land surface elevation to the water table elevation (WTE) after Peck and Payne (2003), with the added criteria of WTE equal to sea level at the shoreline:

$$\mathrm{WTE} = a * \mathrm{LSE} \quad (3)$$

where a is 0.933 ($n = 328$, $R^2 = 0.97$) and 0.911 ($n = 302$, $R^2 = 0.99$) for the wet and dry seasons, respectively. The estimated baseline water table depth fluctuates seasonally from zero at sea level to 3.5 m at the study area's maximum elevation (158 m; Figure 1).

2.2.5. Debris Flow and Avalanche Runout Relationship

Where robust landslide inventories exist, the global runout relationships in Pollock and Wartman (2025) can be replaced by relationships that reflect the local geology and topography. Baum et al. (2000) mapped over 200 shallow flowslides and debris flows triggered during the winters of 1996–1997 along a 40 km stretch of coastline immediately north of Seattle. Using the mapped landslide polygons, we estimated landslide volume (V, m^3) using an area-volume scaling relationship for soil landslides in Oregon and Washington (Larsen et al., 2010). We measured the total runout length (L, m) along a straight line from headscarp to toe. Following Pollock (2020), we produced the ordinary least squares (OLS) regression runout relationship ($n = 250$):

$$\log(L) = 0.2976 * \log V + 0.8120 \quad (4)$$

with a standard deviation of residuals of 0.113, and $R^2 = 0.74$.

2.2.6. Elements at Risk

We considered landslide risk to structures and their occupants using the City of Seattle building inventory (Seattle GeoData, 2018a) and census tract population from the 2017 5-year American Community Survey (ACS; U.S. Census Bureau, 2020). We removed unoccupied structural additions such as decks, patios, and garages from the

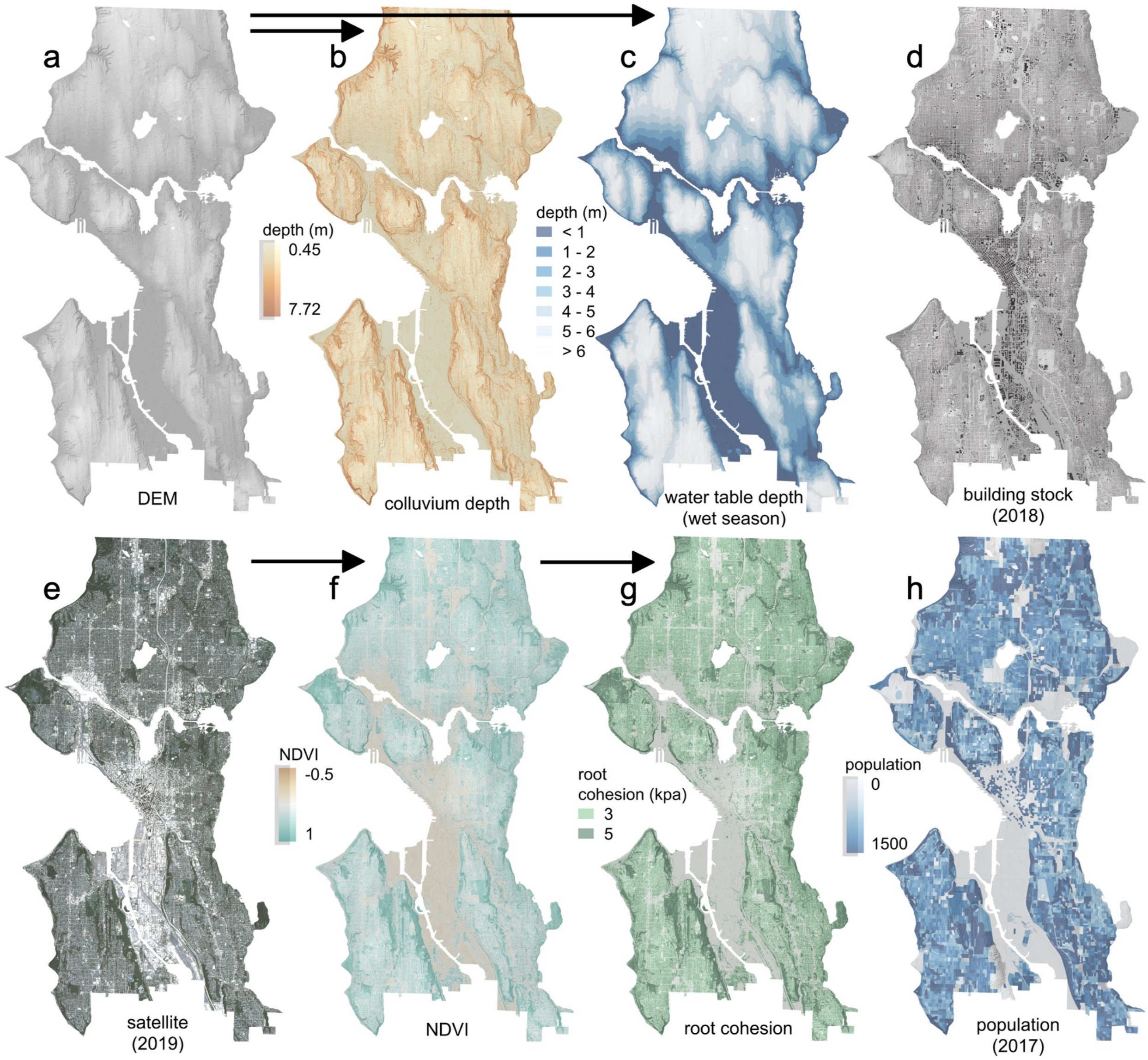

Figure 1. Spatial inputs to MM_3: (a) Digital elevation model (DEM; Quantum, 2016), (b) colluvium depth based on topographic slope, (c) initial wet (winter) season water table depth, (d) 2015 Seattle building stock, (e) satellite imagery, (f) normalized difference vegetation index (NDVI), (g) root cohesion, and (h) 2017 American Community Survey population estimate. Arrows indicate processing workflows where subsequent layers are derived from preceding data.

inventory based on embedded attributes. Tax parcel data provided information on the construction material, size, usage, number of bedrooms, and appraised value of buildings (King County Department of Assessments, 2020).

To assign asset values and resident population from tract and parcel scale to individual building footprints, we assumed that (a) the resident population among tax parcels is proportional to the number of bedrooms, and (b) the distribution of both the resident population and the value among buildings on a given tax parcel is proportional to building footprint area. Individuals above the ground floor of a building are significantly less likely to be injured or killed during a landslide (Pollock & Wartman, 2020). In this study, we consider only the population on the ground floor to be at risk from landslides. An individual's exposure to landslides depends on movement patterns in and out of hazardous areas. Most of Seattle's business zones are on coastal flats and low-relief uplands, while its residential areas occupy the steep and landslide-prone waterfront bluffs. We adopted a fixed exposure value of 0.65, representing the estimated proportion of time individuals will spend at home throughout a year, consistent with long-term international averages (Khajehzadeh & Vale, 2017). This methodology assumes the at-risk population is entirely indoors at their residence and that monetary damage applies only to major structures, excluding outbuildings (sheds, decks, etc.), utilities, vehicles, or land devaluation.

2.2.7. Precipitation Triggering

Precipitation is the most common trigger of landslides in the region, with 91% of all landslides occurring during the wet winter season from November-April. Seattle's slopes are most susceptible to shallow landslides at 1- to 3-day rainfall durations (Chleborad, 2000; Godt, 2004; Godt et al., 2006; Laprade et al., 2000; Salciarini et al., 2008; Tubbs, 1974). Deep-seated landslides are sensitive to longer duration and antecedent rainfall (Miller, 2016; Van Asch et al., 1999) and typically occur days to months after intense precipitation (Wait, 2001). However, probabilistically modeling this relationship requires both site-specific information about the hydrogeology of individual landslide-prone slopes and probabilistic antecedent rainfall curves, neither of which are available for Seattle. We modeled transient groundwater triggering using the baseline of average wet-season groundwater depth (Section 2.2.4) and 3-day rainfall values from Seattle Public Utilities' intensity-duration frequency curves (Rath et al., 2017; Figure S3 in Supporting Information S1). We modeled six rainfall intensities between the 10- and 1,000-year return-period values, which ranged from 0.16 to 0.30 cm per hour (Table S5 in Supporting Information S1). Starting from the initial groundwater table from Section 2.2.4, we used the program TRIGRS (Baum, Godt, & Highland, 2008; Baum, Savage, & Godt, 2008) to simulate groundwater rise as precipitation infiltrates through an unsaturated-saturated soil profile, as described in Pollock and Wartman (2025). Excess surface runoff is routed from less permeable terrain pixels to more permeable pixels downslope, although this does not account for site-specific anthropogenic drainage modifications (e.g., roadways, rooftops, stormwater systems). Soil hydrologic parameters are provided in Table S3 in Supporting Information S1.

2.2.8. Seismic Triggering

We used the peak ground accelerations (PGAs) at return periods of 224, 308, 391, 475, and 975 years from the 2018 update to the National Seismic Hazard Map (USGS, 2018; see Figure S4 in Supporting Information S1). The PGAs represent the aggregation of potential earthquake sources, severities, and likelihoods rather than specific scenario events.

2.2.9. Scenario Combination

We computed the probability of landslide initiation (source zones) and impact (runout zones) for shallow soil slides, debris falls, and rotational slumps under each triggering scenario using the mode-specific stability and runout modules of MM_3 (Pollock & Wartman, 2025). Adjacent failing pixels (FS < 1) are clustered to create synthetic landslide source zones with unique attributes (e.g., volume, areal extent) to initialize the runout model (Text S3 in Supporting Information S1). Figures S5 and S6 in Supporting Information S1 show example source and runout zones, respectively, for each mode in a single Monte Carlo realization. We used a Monte Carlo approach to account for uncertainty in material and model parameters with 500 simulations for each precipitation scenario and 250 simulations for each seismic scenario, split between wet- and dry-season groundwater conditions. Tables S3 and S4 in Supporting Information S1 provide the probability distributions of parameters.

3. Results

3.1. Probabilistic Landslide Hazard

Hazard is concentrated along Seattle's coastal bluffs and inland bodies of water, with peak annual hazard in northern Seattle (Carkeek and Golden Gardens Parks), central Seattle (Discovery Park and Queen Anne Greenbelt), and southwest Seattle (Alki Point and Arroyos Natural Area) (Figure S7 in Supporting Information S1). Not incidentally, many of Seattle's parks and green spaces have been preserved from development because of their unstable slopes (Williams, 2015).

Seattle's historical landslide inventory provides a first-order verification of MM_3's predictive ability. Forty-two percent of inventoried landslides fall above annual probabilities of 1×10^{-4} (i.e., 1 in 10,000), and 28% fall between annual probabilities of 1×10^{-5}–1×10^{-4}. Twenty-two percent fall outside of zones of substantive hazard, but this may be due to address-based rather than slope-based geolocation of landslide points in the

Table 1
The Relative Severity of Shallow Landsliding in Different Return-Period Triggering Scenarios and Groundwater Conditions

Trigger	Groundwater conditions	Return period (yr.)	Number of landslides	Cumulative source area (km^2)	Total area (km^2)
Precipitation	Wet	10	238	0.015	0.111
		50	287	0.018	0.135
		500	344	0.020	0.153
		1,000	328	0.020	0.145
Seismic	Dry	475	2,889	0.300	1.437
		975	7,542	0.929	4.534
	Wet	475	3,921	0.504	2.442
		975	8,801	1.308	6.278

Note. Average values are given.

inventory and the large percentage (52%) with documented human influence that contributes to landslides occurring in otherwise unsusceptible terrain.

3.2. Influence of Seasonality and Trigger Type

Wet-season conditions increase the area impacted by coseismic shallow landslides by 40% (975-year return period) and 70% (475-year return period) over dry-season conditions, with over 1,000 additional landslides for both scenarios (Table 1). The 975-year scenario, corresponding to PGA of 0.4–0.5 g throughout Seattle, generates almost 9,000 shallow landslides under wet-season conditions, although this ranges up to 17,000 landslides in the most severe model realization.

Precipitation triggers fewer shallow landslides than seismic shaking at comparable return periods, with 740–1,040% more landslides under 475-year shaking than in the 500-year rainfall (Table 1). Precipitation-induced landslides are also smaller, averaging 443 m^2 per landslide (about the size of Seattle's average residential lot) compared to 497 and 623 m^2 under dry- and wet-season seismic triggering, respectively. Unlike coseismic landsliding, precipitation-induced landsliding appears to saturate, with the total shallow landslide area plateauing at about 0.15 km^2 for long-return-period rainfall.

Figure 2 highlights different spatial signatures of landslide hazard under precipitation and seismic triggering above Alki Avenue in West Seattle. Under 500-year rainfall, shallow landslides hazard is low (1%–2%) but widespread across coastal bluffs and drainages (Figure 2d). Under 475-year shaking, the probability of impact reaches 80%–90% under wet conditions, concentrated below a high-relief, mid-slope bench (Figure 2b). Dry-season conditions produce a similar spatial hazard pattern, but with about 10% lower probability of impact. The spatial pattern of hazard from rotational slumps is similar across the scenarios, except for two high probability (60%–70%) zones that develop under seismic conditions (Figures 2a and 2e).

3.3. Probabilistic Landslide Risk

The predicted landslide risk in Seattle is substantial: about 18 landslide fatalities and $47 million in structural damage annually. Precipitation-induced landslides contribute 62% and 70% of risk to humans and structures, respectively (Table 2). Shallow landslides dominate Seattle's risk profile at 99% of human fatalities and 97%–99% of structural damage across all modes. Coseismic rotational slumps and debris falls contribute up to 1.7% and 1.0% of structural losses, respectively, depending on the groundwater conditions.

Figure 3 shows the spatial distribution of landslide risk for humans and structures, aggregated by census block. Structural risk is concentrated, with hotspots along Alki Avenue, Harbor Avenue, Westlake, and South Lake Union (Figure 3a). With the exception of Alki Avenue, these locations have relatively low annual hazard, but a high annual risk, due to their expensive business and residential complexes. Human risk is widespread, distributed across Seattle's hillside residential areas, including along the Puget Sound, Lake Washington, and Queen Anne (Figure 3b).

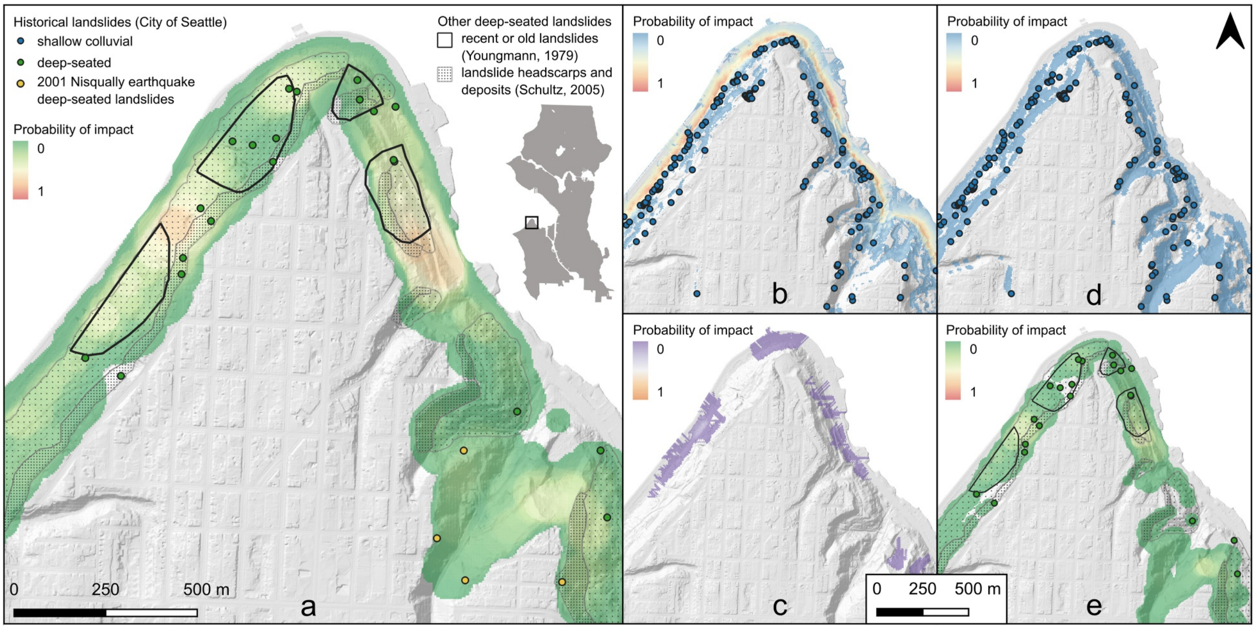

Figure 2. Annual probability of landslide impact at Alki Point in the wet-season 475-year seismic scenario (a–c) and the 500-year rainfall scenario (d and e) from each mode of landsliding: deep-seated slumps (a and e), shallow colluvial slides (b and d) and debris falls (c). No debris falls were triggered in the 500-year rainfall scenario.

Elevated landslide risk occurs in many of the same landslide-prone locations highlighted in previous landslide susceptibility and hazards studies (e.g., Allstadt et al., 2013; Coe et al., 2000; Grant, 2017; Harp et al., 2006). These include along Alki Avenue, the western margin of the Duwamish waterway, coastal bluffs below Magnolia Avenue, the southwest and northeast slopes of Queen Anne, and near Arroyos Natural Area in South Seattle. However, examining landslide risk adds important information otherwise missed in susceptibility and hazard studies, and our results highlight the often nonlinear relationship between landslide hazard and risk. While historical landslide hazard at Carkeek Park has been relatively high, prompting costly projects to drain the hillslopes (Allstadt et al., 2013; Harp et al., 2006; Laprade et al., 2000; Wait, 2001), the risk to humans and structures is relatively low. Similarly, other "problem" areas historically associated with elevated landslide hazard, such as the north end of Magnolia bluff, Ravenna, South Beacon Hill, and the inland drainages of West Seattle (Coe et al., 2004; Godt, Baum, et al., 2008; Harp et al., 2006), have low risk due to low population density. Conversely, susceptibility and hazard maps do not communicate the disproportionately high risk of areas such as southwest Queen Anne and Westlake, which is driven by their dense population and high building values.

Table 2
Total Annual Risk to Humans and Structures in Seattle

Element at risk	Trigger	Annualized risk (yr^{-1})	Percent
Humans	Precipitation	11.2	62.1
	Seismic	6.9	37.9
	Total	18.1 lives	
Structures	Precipitation	32.5	69.5
	Seismic	14.2	30.5
	Total	46.7 $M (2020 USD)	

Note. Average values are given.

MM_3 estimates risk at the level of individual buildings. Figure 4 overlays annualized structural risk with mapped historical landslides and field observations for two locations in Seattle. Historical data provides a first-order independent verification of the spatial distribution (if not magnitude) of building-level risk: an accurate model should identify where historical landslides impacted existing structures. Figure 4a shows a deep-seated landslide that was reactivated by heavy precipitation in 1997 (Laprade et al., 2000; Youngmann, 1979). Offsets in structure foundations and repeatedly patched pavement indicate episodic movement across the headscarp (Figure 4, images a1 and a2). Figure 4b shows estimated risk at both the crest and toe of a coastal bluff that has experienced recent shallow slides, including one that occurred from the deposit of a larger failure shortly before image b1 was taken. To the southeast, a series of homes has been repeatedly damaged by shallow slides originating from the crest of the bluff (Seattle GeoData, 2023).

10.1029/2025EF007594

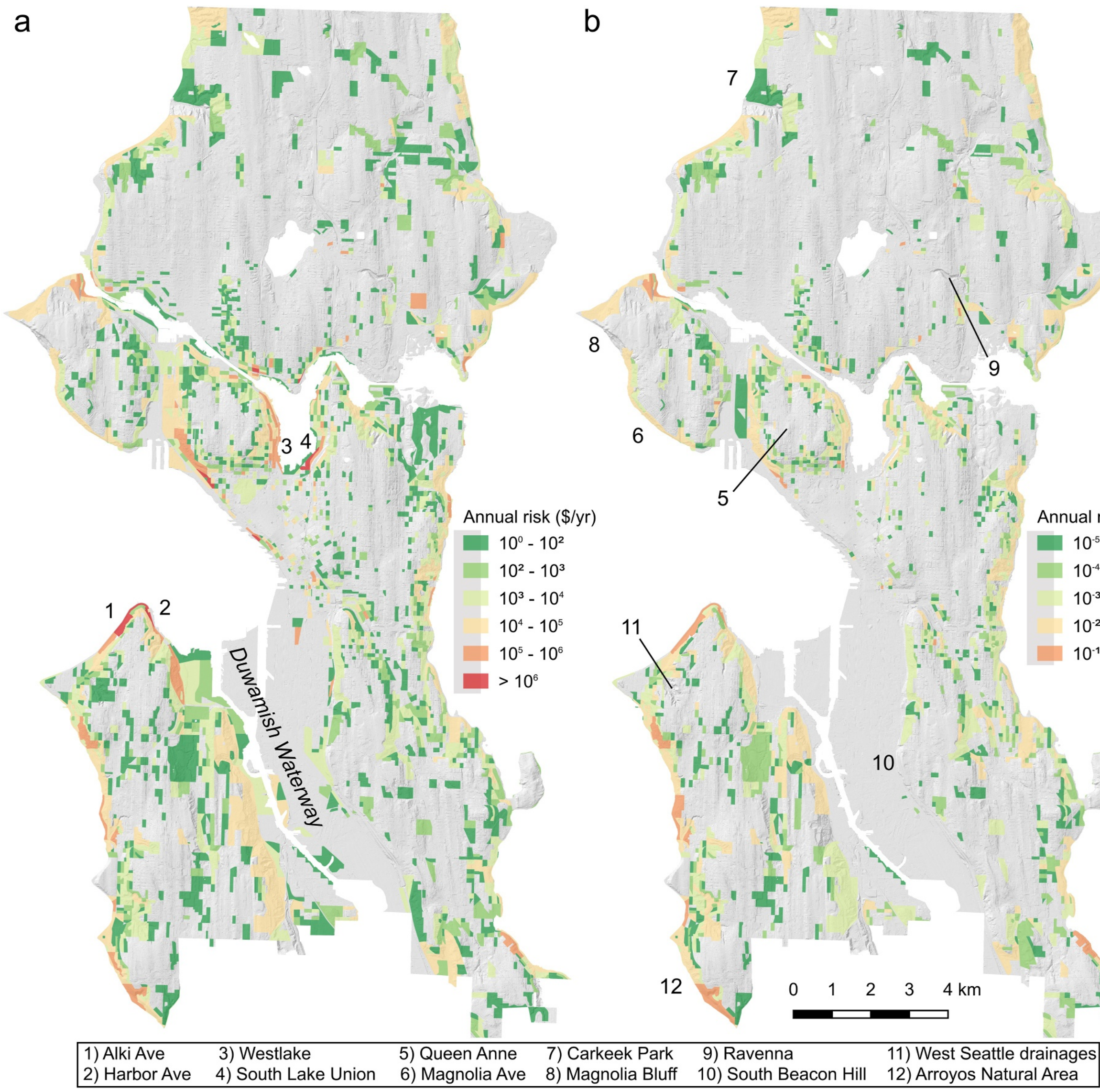

Figure 3. Annual risk aggregated by census block considering (a) structural damage and (b) human loss of life.

4. Discussion

4.1. Disaggregation of Landslide Hazard and Risk

MM_3 facilitates the creation of *risk profiles* (Strouth & McDougall, 2022) by disaggregating total landslide risk into its component parts, including relative contributions of hazard, exposure, and vulnerability, and between landslide modes, triggering events, and return-period scenarios. In Seattle, short-return-period precipitation-induced landslides dominate the cumulative annualized hazard, exposure, and risk (Figure 5). These components of risk can interact counterintuitively as a function of landslide location and size. At comparable return periods, the annualized area impacted by coseismic landslides is up to 45 times higher than for precipitation-induced landslides, but the associated contribution of exposed buildings and people is lower due to sparser development in impacted areas (Figures 5a, 5c, and 5d). However, individual coseismic landslides are on average larger and more damaging, maintaining their outsized influence on annualized risk at comparable return periods (Figures 5e and 5f). While the low frequency of extreme precipitation events mutes their annualized risk contribution, seismic triggering events show the opposite trend. The rising tail of the annualized risk curve for

10.1029/2025EF007594

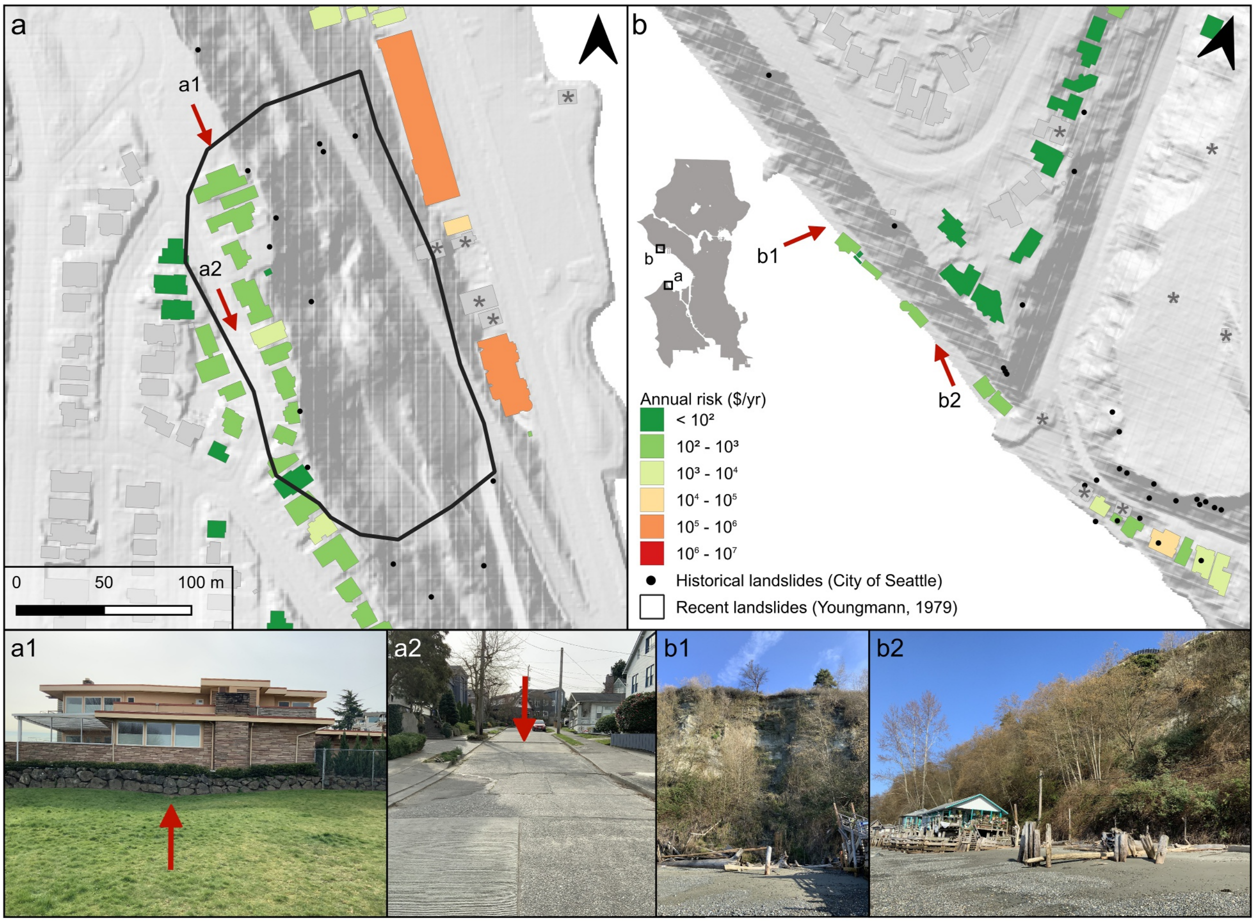

Figure 4. Estimates of average annual structural risk along two coastal bluffs in Seattle. Red arrows correspond to camera positions for images a1–b2. Negligible mapped risk for buildings marked with "*" is due to missing structural value data in the building inventory rather than an absence of hazard.

seismic events suggests that the unquantified risk for very large seismic events (i.e., return periods greater than 1,000 years) is significant and warrants further investigation (Figures 5e and 5f).

Figure 6 shows risk in absolute rather than annualized terms, highlighting the inverse proportionality between the consequences and frequency of seismic triggering events. Strong ground shaking with an approximately 975-year return period could expose over 12,000 structures and 60,000 residents to landslides (Figures 6c and 6d). The slight flattening of the seismic hazard curves at low return periods (Figures 6a and 6b) suggests a drop-off in the number of triggered landslides toward a baseline of terrain pixels that are marginally stable under static conditions (i.e., FS ~1.0 using mean input parameters and without the effect of precipitation or seismic shaking). In the model space, these pixels will "fail" in a proportion of Monte Carlo realizations due to parameter sampling, regardless of the presence of a trigger, corresponding to a background rate of landsliding. Including additional seismic triggering scenarios at the upper and lower ends of the temporal range (below the 224-year return period and above the 975-year return period) could provide insight into a minimum PGA to trigger coseismic landslides (Jibson & Harp, 2016) and the apparent linear scaling of hazard and risk for severe ground shaking. Precipitation-induced hazard and risk saturate around the 100-year rainfall intensity. We interpret this to reflect an intensity threshold, above which surface water is routed downslope as runoff rather than infiltrating into the soil column, thus triggering few additional landslides. Counterintuitively, approximately 200 more buildings are exposed to landslides in the 10-year scenario than in the 25-year scenario (Figure 6d), demonstrating some Monte Carlo instability influencing the spatial distribution of landslides at low return periods. This is due to our definition of exposure and modeling artifacts. We count a structure (or resident population) as "exposed" to landslides if it intersects with an area of nonzero hazard (even if the hazard is very low). Thus, while the hazard and risk measures in Figure 6 are averages across all Monte Carlo realizations and converge rapidly (see Text S5 and

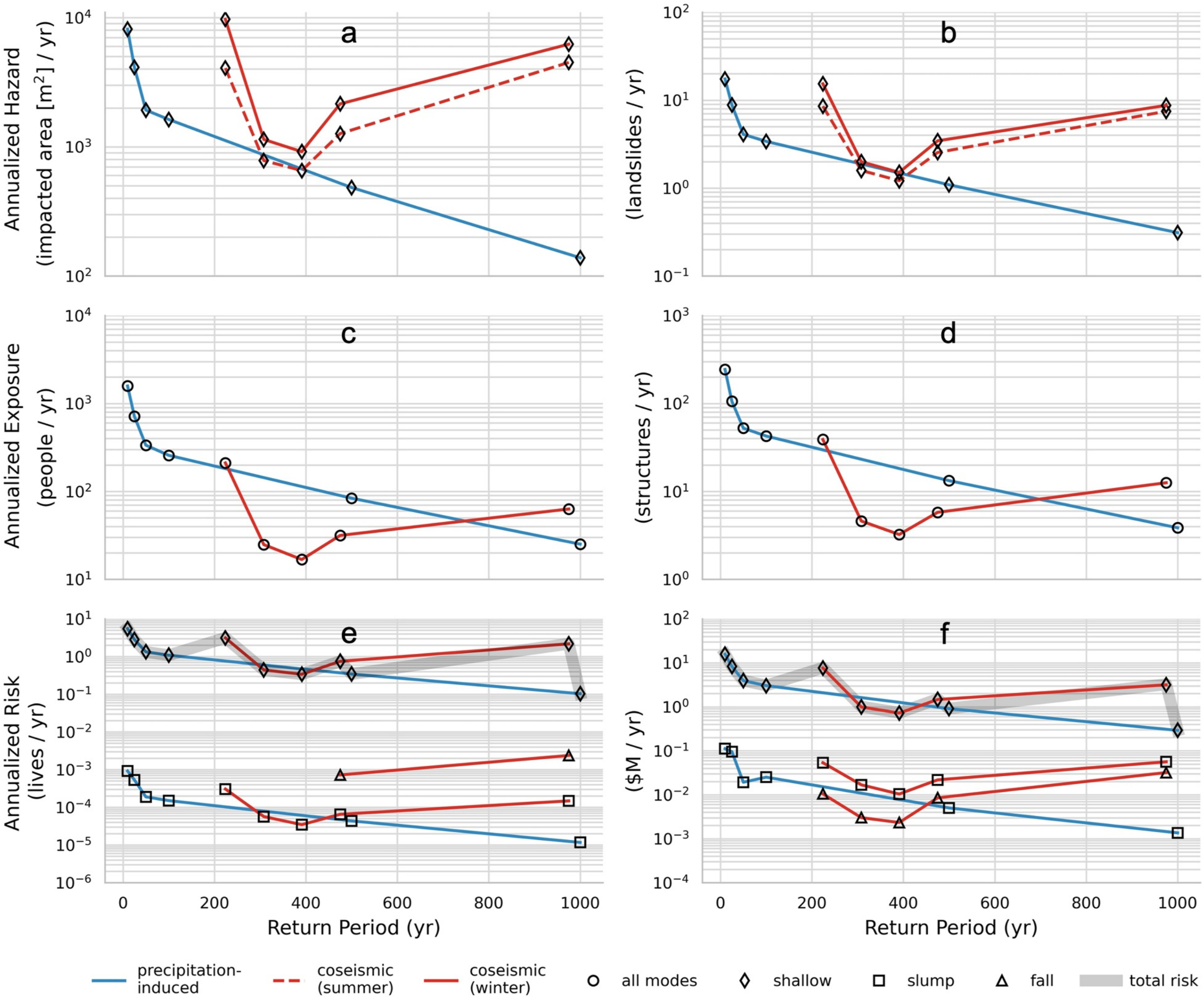

Figure 5. Annualized hazard, exposure, and risk curves for precipitation-induced landslides (blue) and coseismic landslides (red). Top: The annualized total hazard measured in area affected by landslides (a) and number of triggered landslides (b). Impacted area and number of landslides only consider the shallow mode. Dashed lines indicate dry season conditions, while wet season conditions are shown with solid lines. Wet and dry groundwater conditions are combined in the other plots. Middle: The annualized exposure to all landslide modes for humans (c) and structures (d). Bottom: The annualized risk from landslides for humans (e) and structures (f).

Figures S10–S12 in Supporting Information S1), exposure is governed by the extreme (worst case) outcomes, which require a greater number of iterations to stabilize. The sensitivity of exposure to the number of simulations is mitigated at higher return periods, where slope stability is increasingly driven by external loading (precipitation, seismic shaking) compared to model "noise" from parameter sampling.

Risk at the scale of individual buildings is strongly influenced by position along the hillslope profile. Figure 7 shows the annualized structural risk on a per-building basis for the Alki area of West Seattle. Most of the structural risk at building (b) at the toe of the slope comes from shallow landslides, split between precipitation (16%) and seismic (63%) triggers (Figure 8b). The other modes contribute substantially to the structural risk, at 11% and 10% for slumps and debris falls, respectively. The dominance of shallow landslides in the structural and human risk of building (b) reflects its location in the runout zone of landslides initiating from a high-relief, mid-slope bench, as well as the relatively high vulnerability of humans and structures to shallow, rapid landslides. One hundred meters up the slope, 68% of structural risk at building (a) comes from precipitation-induced slumps undercutting the slope crest while only 4% comes from shallow landslides. However, due to the relatively low human vulnerability to slumps, 89% of the human risk at building (a) comes from infrequent shallow coseismic

10.1029/2025EF007594

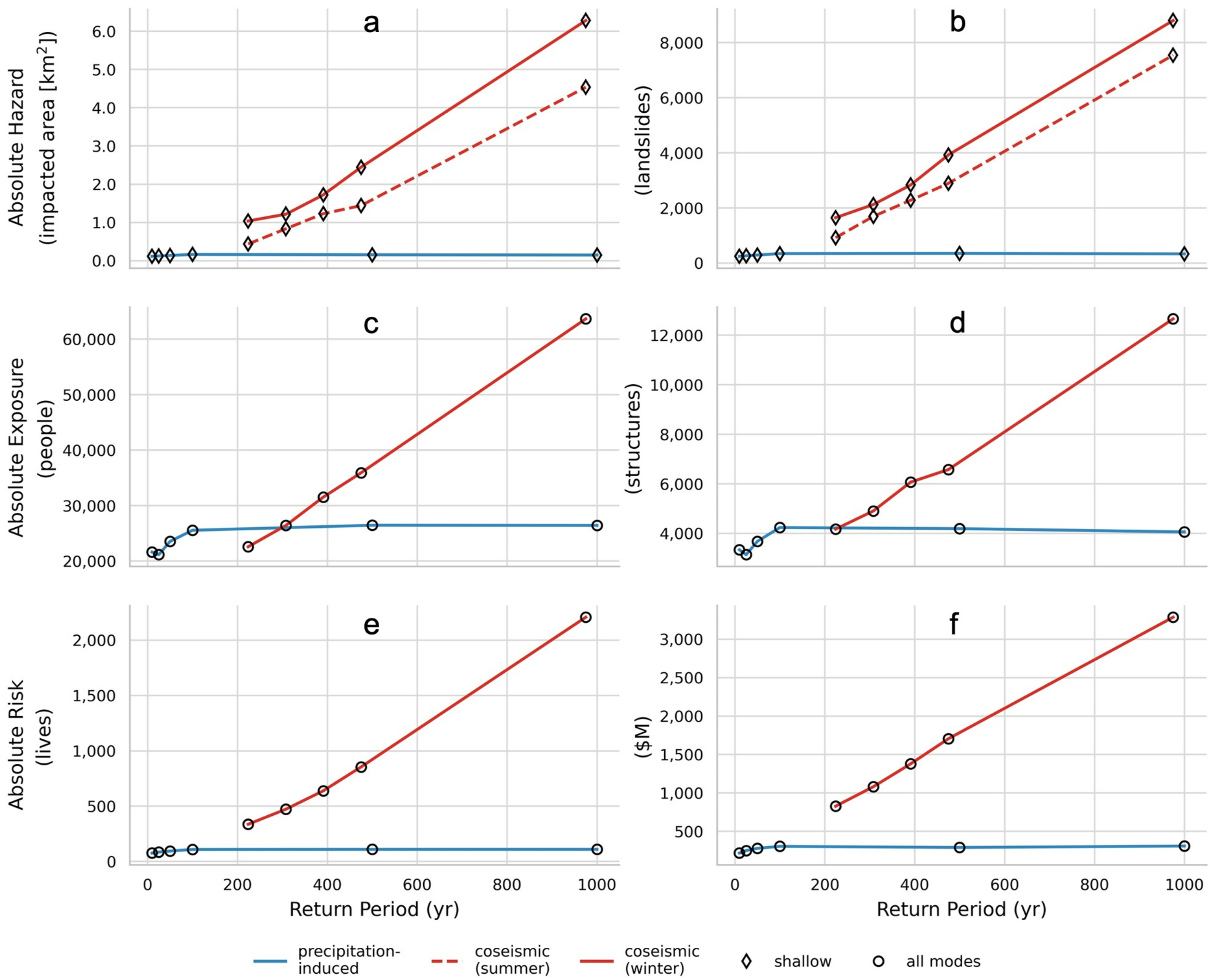

Figure 6. Absolute hazard, exposure, and risk curves for precipitation-induced landslides (blue) and coseismic landslides (red). Top: The absolute total hazard measured in area affected by landslides (a) and number of triggered landslides (b). Impacted area and number of landslides only consider the shallow mode. Dashed line indicates dry-season conditions, while wet-seasons conditions are shown with the solid line. Wet and dry groundwater conditions are combined in the other plots. Middle: The absolute exposure to all landslide modes for humans (c) and structures (d). Bottom: The absolute risk from landslides for humans (e) and structures (f).

landsliding (Figure 8a). Disaggregated risk such as that shown in Figure 8 facilitates the tailoring of building design and mitigation measures to the primary drivers of risk at each location.

4.2. Comparison With Historical Landslide Damage

No systematic record of landslide fatalities in Seattle currently exists. We compiled an inventory of 16 landslide fatalities within Seattle city limits from a non-exhaustive review of regional newspaper archives (Table S6 in Supporting Information S1). The annual landslide fatality rate peaked in the 1920s and 1930s, between 8.40×10^{-4} and 1.11×10^{-3} per thousand people. At Seattle's 2017 population, this would translate to a fatality every 15–24 months (Table S7 in Supporting Information S1). We found conclusive records of only one landslide fatality since 1940, suggesting a changing landslide risk regime that coincides with the City's shift to proactive landslide management starting in 1933 (Laprade, 2007).

Estimated annualized risk in this study is orders of magnitude greater than recorded, albeit incomplete, historical landslide losses. This is in part because Seattle has not experienced many of the triggering conditions modeled in this study in the recent (recorded) past. Since 1948, only one rainfall event exceeded the 50-year intensity modeled in this study, as measured at Seattle-Tacoma International Airport (NOAA, 2024). In the last century, Seattle has experienced five notable earthquakes (1939, 1946, 1949, 1965, 2001), but with the exception of the

10.1029/2025EF007594

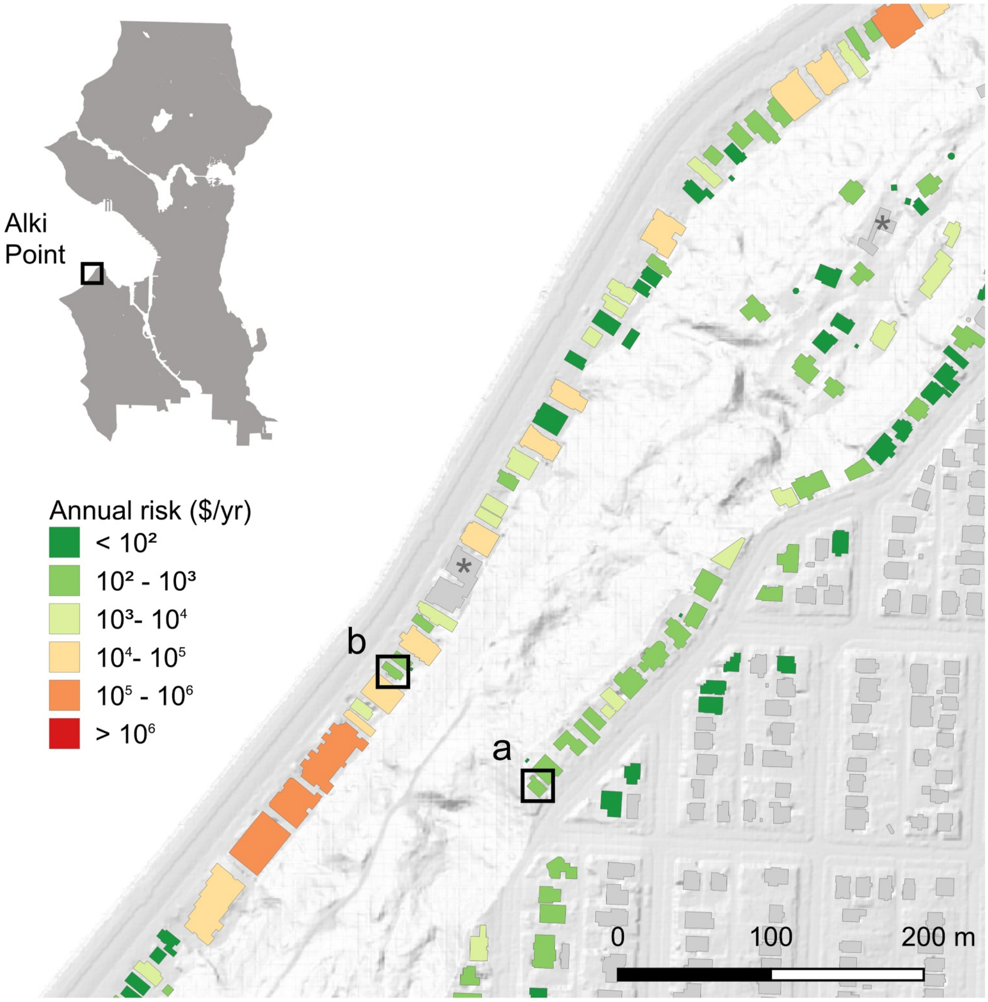

Figure 7. Average annual structural risk in the Alki area of West Seattle. MM_3 disaggregates risk into the unique contributions from different modes and triggers at each structure, as shown in Figure 8 for buildings (a) and (b). Negligible mapped risk for buildings marked with "*" is due to missing structural value data in the building inventory rather than an absence of hazard.

2001 Nisqually earthquake, these caused minor landslide damage (Chleborad & Schuster, 1990; Highland, 2003). PGA in the Nisqually earthquake was around 0.1 g throughout the city, lower than the 224-year shaking intensity considered in this study. We note that return periods are long term averages; in the near-term, a "10-year return-period" event could reoccur over a longer (or shorter) interval than 10 years. Limitations of historical records notwithstanding, we identify five primary reasons for methodological overprediction of risk:

1. *Direct landslide mitigation.* Since 1933, the City of Seattle has undertaken numerous slope stability improvement projects (Laprade et al., 2000). MM_3 does not account for direct landslide mitigation, except incidentally insofar as it alters the underlying terrain data (e.g., regrading). As such, our results represent the potential landslide risk in Seattle in the absence of mitigation.
2. *Anthropogenic terrain modification.* Widespread human modifications—including retaining walls, building foundations, impervious surfaces, and stormwater drainage systems—alter landslide hazards, with some features stabilizing slopes and others destabilizing them. These anthropogenic modifications can lead to landslide overprediction (Coe et al., 2000).
3. *Model simplification.* The physically-based models of MM_3 trend toward conservatism by (generally) neglecting stabilizing side forces. For instance, shallow infinite-slope failure models are conservative in most cases (Griffiths et al., 2011). Additionally, applying idealized hillslope models to individual pixels tends to

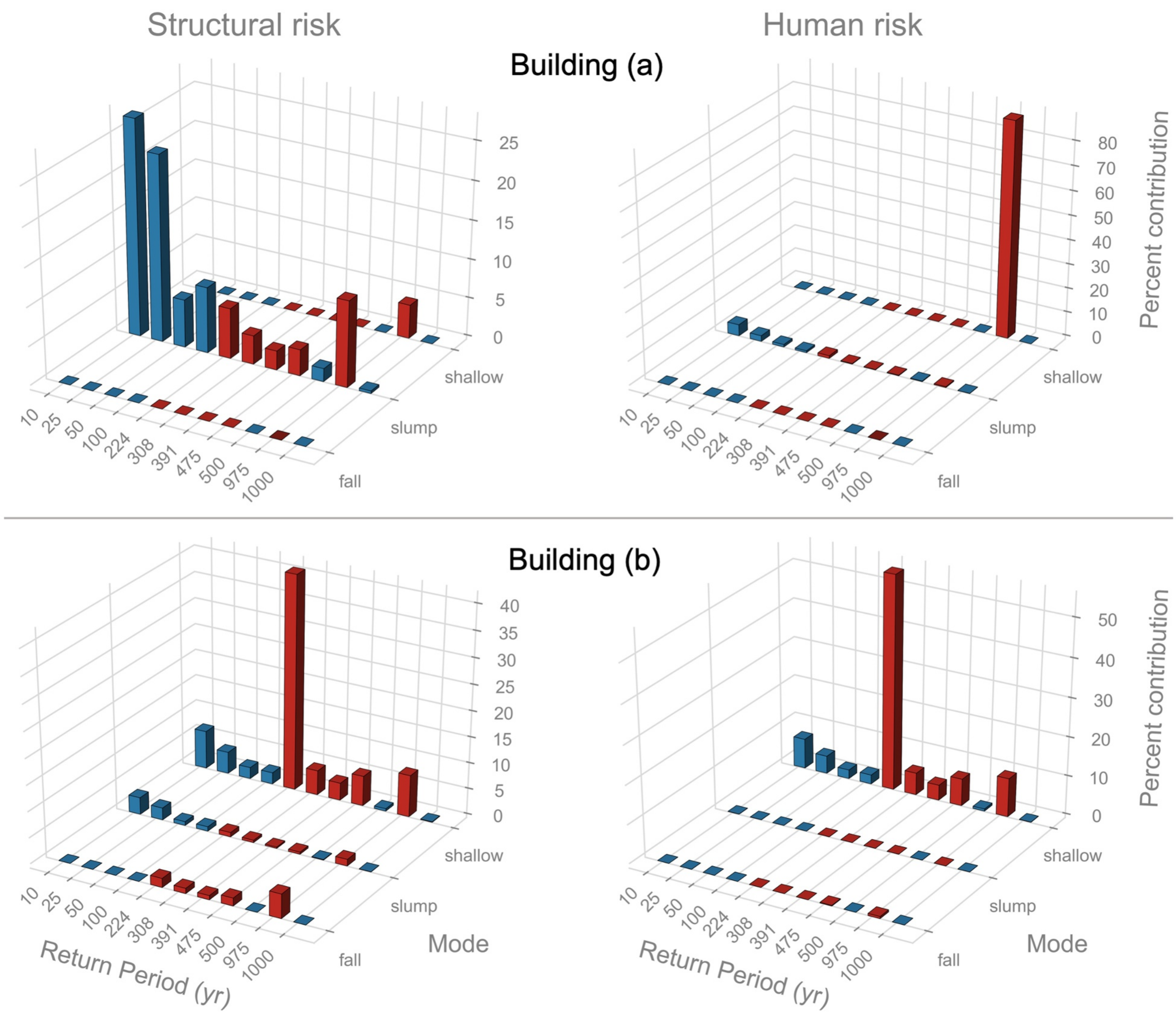

Figure 8. Annual risk disaggregation for buildings (a) and (b) in Figure 7. Return-period triggering events associated with precipitation (blue) and seismicity (red) are shown on the lower left axis while the landslide modes are shown on the lower right. Percent contributions are with respect to the total annual risk for each building.

overestimate landslide volume, which is compounded in subsequent volume-driven estimates of runout and vulnerability.

4. *Human evasion.* The ability of humans to notice and evade approaching landslides significantly reduces vulnerability but lies beyond the science's current ability to model for PLRA (Pollock & Wartman, 2020). Our review of Seattle's landslide fatalities noted many reports of residents surviving landslides by evasion of oncoming debris or precautionary evacuation (e.g., Maier, 1997). In the events listed in Table S6 in Supporting Information S1, an average of 2–3 individuals escaped for each one who was killed.
5. *Sparse vulnerability data.* Seattle's rapid urban densification has replaced many of its single-family timber homes with concrete multifamily housing, especially in landslide-prone areas. Existing vulnerability curves for shallow landslides are generally derived from databases of single-family residences which have lower resistance to landslides than multistory, dense urban architecture (Ciurean et al., 2017).

These limitations are common to regional-scale landslide risk analyses (as well as many local studies) and represent areas of needed research. Additionally, building-scale risk estimates based on regional data sets are inherently uncertain. Although in this work we use average, "best estimate" risk values to demonstrate the MM_3 framework, MM_3 natively estimates risk as a range by propagating input uncertainty through a Monte Carlo approach. Quantified risk uncertainty bounds, even if large, can be transparently communicated and incorporated into risk management decisions (Strouth & McDougall, 2022). MM_3 is designed as a regional-scale screening tool to guide and complement, rather than replace, site-specific studies and local engineering experience.

4.3. Implications for Land Use Policy

In 2006, the City of Seattle codified portions of the susceptibility maps produced by Laprade et al. (2000) into the decision-making process (Miscolta-Cameron, 2016). However, development restrictions in landslide-prone areas are based on landslide susceptibility and do not explicitly include considerations of the timing, runout, or consequences of landslides (Seattle OEM, 2019). Including landslide runout expands the area potentially impacted by landslide by 80% to almost 33 km^2 (Table S8 in Supporting Information S1).

The susceptibility zones of Schulz (2005) and the hazard zones presented in this study cover about 15% of Seattle's land and encompass approximately 23,000 buildings, about twice the number in City-designated landslide-prone areas. Approximately 6,770 buildings have annual risk over $100 per building, but about 58% of these fall outside the City's landslide-prone areas. The most significant spatial differences between the City's landslide-prone areas and the modeled hazard zones come from shallow landslide runout in Interbay, the margins of the Duwamish waterway, the bluffs near Seward Park, and near Arroyos Natural Area (Figure 9). These are locations in which different modes of failure, infrequent but intense triggering events, and post-failure behavior is not represented in the landslide inventory which underpins the City's land use policies. However, we note that no occupied location is wholly without risk, and some level of landslide risk is tolerable in the context of other risky activities that humans engage in daily. The threshold of tolerable risk will vary between communities, hazard types, and individuals (Strouth & McDougall, 2022).

Who holds the risk in Seattle? Individuals with non-negligible landslide risk are typically whiter and wealthier (as proxied by property value) than other Seattle residents. The median value of a moderate risk property (annualized risk greater than $100) is 85% higher than the median for all Seattle, reflecting the premium placed on slope-proximal waterfront and skyline-view homes. However, among moderate risk properties, property value is weakly correlated to both structural and human risk (R^2 of 0.069 and 0.058, respectively), suggesting that social stratification away from higher-risk areas is not occurring as widely in Seattle as it does elsewhere (Santi et al., 2011). Possible reasons include a short collective recollection of hazard, overreliance on municipal regulation of slope development, or de-prioritization of risk avoidance in the context of competing values (e.g., aesthetics, neighborhood reputation, social networks, etc.; Miscolta-Cameron, 2016). The distribution of landslide risk generally follows the racial makeup of Seattle at census-tract level, with those individuals self-identifying as white holding only slightly more risk relative to population (71.4% of at-risk individuals compared to 68.6% of the population). Black and Asian residents are 1.2% and 1.7% less likely, respectively, to hold landslide risk than demographics would suggest.

Mapping risk provides additional information missed in susceptibility analyses. While the current landslide-prone areas (*susceptibility*) treat all landslide areas equally, risk mapping demonstrates that some regions of Seattle are disproportionately affected by landslides. The Central Seattle neighborhoods of Westlake, and East, North, and Lower Queen Anne cumulatively hold 16% and 23% of the human and structural risk, respectively, yet only 6.3% of the designated landslide-prone land. Meanwhile the Delridge neighborhoods of Riverview and Highland Park have 7.5% of the designated landslide-prone areas, but only 0.2%–0.3% of annual risk for both humans and buildings. Using this example, policies that allocate mitigation funding (or permit development) based on susceptibility maps alone would likely be nonconservative in Central Seattle and disproportionately cautious in Delridge, relative to the actual potential for damage.

4.4. From Landslide Risk to Land Use Policy

The number of fatal landslides globally surged by over 90% in 2024 and over 20% in the first half of 2025 compared to the historical mean, coincident with some of the warmest surface temperatures on record (Froude & Petley, 2018; Petley, 2025a, 2025b). Climate change's full influence on landslide incidence remains unclear, but these preliminary observations highlight the urgent need for forward-looking, physically-based PLRA that incorporates projected future conditions, rather than solely relying on historical landslide rates. MM_3 represents one such tool for risk-based land use decision-making, planning, and sustainable land management in the dynamic, human-environment ecosystem of the Anthropocene. Although this study focuses on Seattle, Washington, MM_3 is readily transferable due to its physical basis, remote-sensing derived inputs, and independence from local

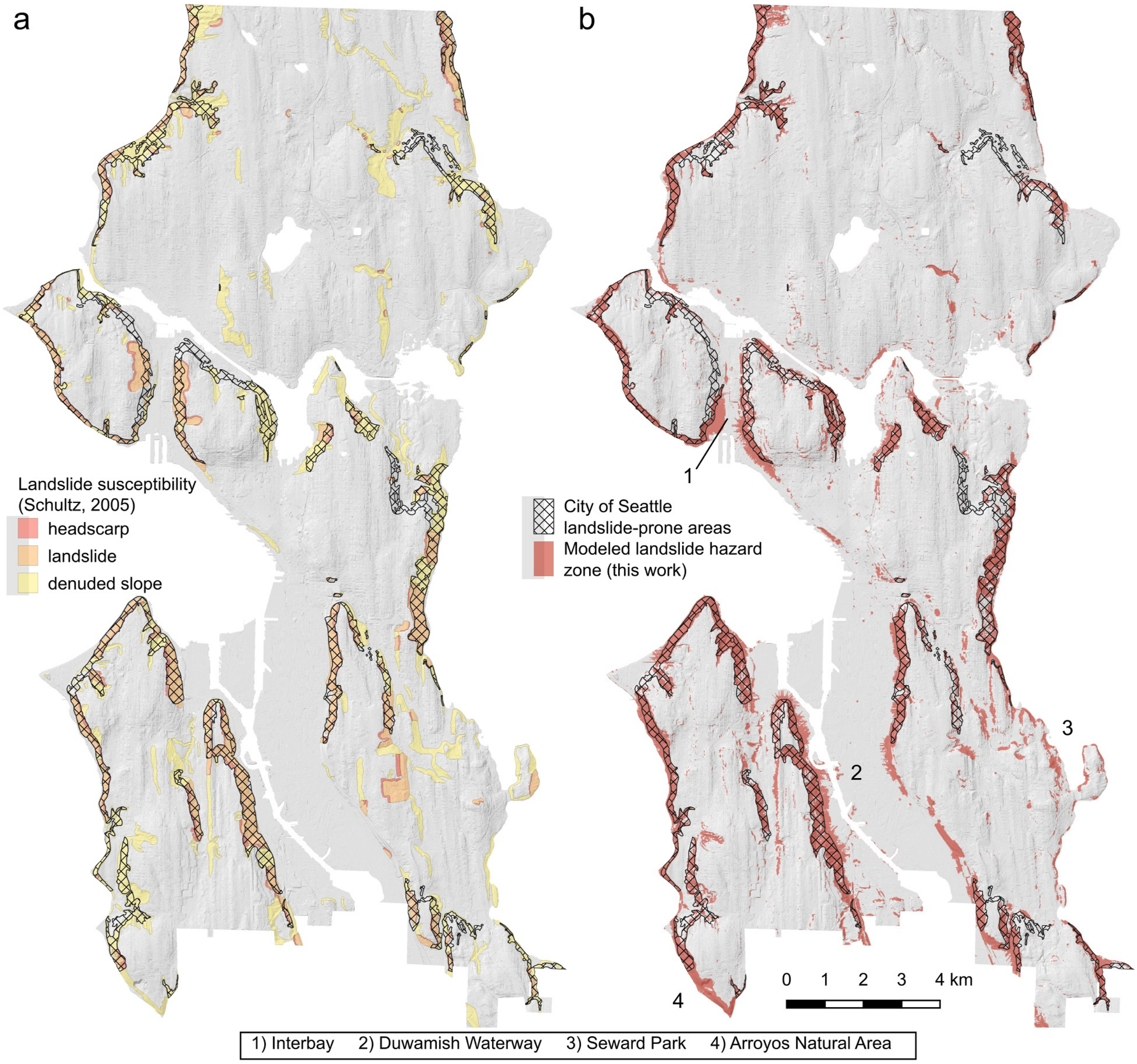

Figure 9. (a) Landslide susceptibility mapping of Schulz (2005) and (b) the area exposed to landslide hazard modeled in this study. Landslide-prone areas defined by the City of Seattle (Seattle Geodata, 2018b) are overlain.

landslide records that may be unavailable or incomplete. Satellite imagery, DEMs, and geologic mapping are available globally at increasingly fine resolution. In our experience, material parameter and element-at-risk data sets have been the most challenging inputs to compile. However, we have found that many public works departments (e.g., departments of transportation, municipal engineers) and private consultants maintain data sets of regional parameter ranges for preliminary design analyses. In remote and understudied regions, landslide inventory inversion has been used to derive regional strength parameters (Gallen et al., 2015; Medwedeff et al., 2025; Townsend et al., 2020). Recent near-global data sets of building footprints and human settlement (Microsoft, 2024; Pesaresi et al., 2013) mean that MM_3 can be applied to map risk almost anywhere in the world.

Risk mapping, such as that enabled by MM_3 and demonstrated in this work, is a necessary precursor to challenging technical and social questions of implementation, such as:

- Does public-facing risk mapping at building-scale infringe on personal privacy?
- How should technical—and critical—information about probability and uncertainty be communicated?

- Given the spatial uncertainty of input data, how are risk boundary cases enforced, and how can affected property owners "challenge the line" to update the mapping?
- Should risk mapping be statutory or only informational?
- How is cost shared in a community when damage occurs, even after hazard and risk information is available?

Landslide risk maps alone do not reduce risk. Risk reduction occurs when maps are communicated, understood, and acted upon by a community. Scientific products that are not readily understandable, actionable, and aligned to local priorities risk being ignored or opposed by stakeholders in the decision-making process (Covello & Allen, 1988; Lempert et al., 2023; Mills et al., 2008). Stakeholder disaccord has impeded landslide hazard mapping and risk reduction efforts in Juneau, Alaska (Provant & Carey, 2023); La Conchita, California (Covarrubias, 2015); Sitka, Alaska (Rose, 2021); North Carolina (Dedman, 2014); and even Seattle itself (Miscolta-Cameron, 2016). Primary reasons cited for resistance to hazard mapping include economic concerns about the impact on property value, opaque justification for the boundaries of mapped hazard classes, and rejection of fatalistic vulnerability labels that frame whole neighborhoods as "dangerous" (Izenberg et al., 2022; Provant & Carey, 2023). Furthermore, absence of a transferable model for PLRA at property-by-property granularity is responsible for widespread unavailability of landslide insurance in the United States (Dixon et al., 2023; French, 2016). Without PLRA, most insurers won't underwrite landslide insurance policies, and without insurance available to transfer their risk, residents are reluctant to endorse hazard and risk mapping that could impact the desirability of their property (Izenberg et al., 2022).

Risk disaggregation alone does not resolve these socio-political complexities. However, it enables engineers, scientists, officials, and community members to collaborate more effectively on land use decisions by:

- Putting risk in economic terms, so that stakeholders can understand and compare the *costs* of action and inaction rather than merely identifying a location as "hazardous."
- Profiling the site-specific components of composite risk to reveal *why* risk exists at a location, which engenders confidence in data-driven maps and ordinances.
- Pointing toward solutions that target location-specific drivers of risk, rather than a singular narrative of vulnerability.

5. Conclusions

The absence of practical, regional models for high-resolution PLRA has contributed to tragic human losses from landslides. Disaggregation of landslide risk through PLRA is critical for land use decision-making and effective risk reduction. Through a pilot application in the City of Seattle, Washington, we introduce the MM_3 model for PLRA and demonstrate that high-resolution, regional-scale risk mapping is both realistic and achievable.

We find that frequent, precipitation-induced shallow landslides drive substantial risk in Seattle, but this risk is disproportionately held in several localized zones. Critically, the nature of this risk is mode-specific: the shallow, rapid slides that disproportionately endanger people are distinct from the slower slumps that typically drive structural risk. While risk in some of these areas is driven by elevated hazard, in others it is a function of high property values and a dense urban population, underscoring the often nonlinear and sometimes counterintuitive relationship between where landslides happen and where they cause the most harm. Although only moderately contributing to annual risk, landslides triggered by strong ground shaking, such as that from anticipated large earthquakes on the Seattle Fault and the Cascadia Subduction Zone, could expose over 60,000 people and 12,000 buildings to landslides, potentially resulting in thousands of fatalities and billions of dollars in damage.

Significantly more buildings are at risk than are currently designated as landslide-prone under susceptibility-based statutory mapping, primarily due to landslide runout being excluded. Our risk mapping quantifies—in space and time—the unique risk signatures of different landslide modes for humans and structures, providing more actionable information than susceptibility maps alone. Critically, risk profiles vary dramatically even over short distances, with relatively small changes in location along a slope strongly impacting building-level risk.

While, significant socio-political barriers exist to implementing data-driven landslide risk analysis into regulatory frameworks, MM_3 provides a technical foundation for this transition. By disaggregating risk into its component drivers and expressing consequences in economic and human terms, this approach creates a common, quantified baseline for the complex social negotiation necessary to reduce risk. As climate change intensifies landslide hazards globally, such frameworks are essential for risk-informed land use planning and building resilient communities in hazardous landscapes.

Conflict of Interest

The authors declare no conflicts of interest relevant to this study.

Availability Statement

The data used in this study is available from the referenced sources and the following public data portals: Lidar: https://lidarportal.dnr.wa.gov/ (Search: "King County 2016," DTM download [Quantum Spatial, 2016]); Population: https://data.census.gov/map/160XX00US5363000,5363000$1400000/ACSDT5Y2017/B02001?q=american+community+survey+2017&t=Race+and+Ethnicity&layer=VT_2017_140_00_PY_D1&loc=47.6089,-122.3697,z9.8767 (U.S. Census Bureau, 2020); Building stock: https://data-seattlecitygis.opendata.arcgis.com/datasets/c7265e8e78f14970bf375d9b2259e82a_0/explore?location=47.611149%2C-122.327808%2C10 (Seattle Geodata, 2018a); Subsurface Database: https://geologyportal.dnr.wa.gov/ [Search: "Borehole Information" (Jeschke et al., 2016)]. Methodological details of MM_3 are provided in an open-access methods paper (Pollock & Wartman, 2025).

Acknowledgments
This material is based upon work supported by the National Science Foundation under Grants 2103713 and 2519682. Any opinions, findings, and conclusions or recommendations expressed in this material are those of the authors and do not necessarily reflect the views of the National Science Foundation.

References

Allstadt, K., Vidale, J., & Frankel, A. (2013). A scenario study of seismically induced landsliding in Seattle using broadband synthetic seismograms. *Bulletin of the Seismological Society of America*, *103*(6), 2971–2992. https://doi.org/10.1785/0120130051

Atwater, B., Satoko, M.-R., Kenji, S., Yoshinobu, T., Kazue, U., & Yamaguchi, D. (2005). *The orphan tsunami of 1700; Japanese clues to a parent earthquake in North America*. United States Geological Survey.

Baum, R., Godt, J., & Highland, L. (Eds.). (2008). *Landslides and engineering geology of the Seattle, Washington area*. The Geological Society of America.

Baum, R., Godt, J., & Savage, W. (2010). Estimating the timing and location of shallow rainfall-induced landslides using a model for transient, unsaturated infiltration. *Journal of Geophysical Research*, *115*(F3), F03013. https://doi.org/10.1029/2009JF001321

Baum, R., Harp, E., & Hultman, W. (2000). *Map showing recent and historic landslide activity on coastal bluffs of Puget Sound between Shilshole Bay and Everett, Washington*. Miscellaneous Field Studies Map MF-2346. U.S. Geological Survey.

Baum, R., Savage, W., & Godt, J. (2008). *TRIGRS—A Fortran program for transient rainfall infiltration and grid-based regional slope-stability analysis, version 2.0*. Open-File Report 2008-1159. United States Geological Survey.

Bazzurro, P., & Cornell, C. (1999). Disaggregation of seismic hazard. *Bulletin of the Seismological Society of America*, *82*(2), 501–520. https://doi.org/10.1785/BSSA0890020501

Chleborad, A. (2000). *Preliminary method for anticipating the occurrence of precipitation-induced landslides in Seattle, Washington*. USGS Open-File Report 00-469. U.S. Geological Survey.

Chleborad, A., Baum, R., Godt, J., & Power, P. (2008). A prototype system for forecasting landslides in the Seattle, Washington, area. In R. Baum, J. Godt, & L. Highland (Eds.), *Landslides and engineering geology of the Seattle, Washington area*. The Geological Society of America.

Chleborad, A., & Schuster, R. (1990). *Ground failure associated with the Puget Sound region earthquakes of April 13, 1949, and April 29, 1965*. USGS Open-File Report 90-687. U.S. Geological Survey.

Cislaghi, A., Chiaradia, E., & Bischetti, G. (2017). Including root reinforcement variability in a probabilistic 3D stability model. *Earth Surface Processes and Landforms*, *42*(12), 1789–1806. https://doi.org/10.1002/esp.4127

Ciurean, R., Hussin, H., van Westen, C., Jaboyedoff, M., Nicolet, P., Chen, L., et al. (2017). Multi-scale debris flow vulnerability assessment and direct loss estimation of buildings in the Eastern Italian Alps. *Natural Hazards*, *85*(2), 929–957. https://doi.org/10.1007/s11069-016-2612-6

Coe, J., Michael, J., Crovelli, R., & Savage, W. (2000). *Preliminary map showing landslide densities, mean recurrence intervals, and exceedance probabilities as determined from historic records, Seattle, Washington*. USGS Open-File Report 00-303 online edition. U.S. Geological Survey.

Coe, J., Michael, J., Crovelli, R., & Savage, W. (2004). Probabilistic assessment of precipitation-triggered landslides using historical records of landslide occurrence, Seattle, Washington. *Environmental and Engineering Geoscience*, *10*, 103–122. https://doi.org/10.2113/10.2.103

Cornell, C. (1968). Engineering seismic risk analysis. *Bulletin of the Seismological Society of America*, *58*(5), 1583–1606. https://doi.org/10.1785/BSSA0580051583

Covarrubias, A. (2015). 10 years after fatal mudslide, tiny La Conchita accepts the risks. *LA Times*.

Covello, V., & Allen, F. (1988). *Seven cardinal rules of risk communication*. U.S. Environmental Protection Agency. Retrieved from https://archive.epa.gov/care/web/pdf/7_cardinal_rules.pdf

Crozier, M., & Glade, T. (2005). Landslide hazard and risk: Issues, concepts and approach. In T. Glade, M. Anderson, & M. Crozier (Eds.), *Landslide hazard and risk*. John Wiley & Sons.

Davis, E., Chang, S., Hou, S., Teal, T., Cowell, K., & Garcia-Arceo, S. (2022). A century of landslides in Seattle, Washington: Coalescing and digitizing the City's historic landslide inventories. *Environmental & Engineering Geoscience*, *28*(4), 335–346. https://doi.org/10.2113/EEG-D-21-00097

Dedman, B. (2014). How politics buries science in landslide mapping. *NBC News*.

de Vilder, S., Massey, C., Lukovic, B., Taig, T., & Morgenstern, R. (2022). What drives landslide risk? Disaggregating risk analyses, an example from the Franz Josef Glacier and Fox Glacier valleys, New Zealand. *Natural Hazards and Earth System Sciences*, *22*(7), 2289–2316. https://doi.org/10.5194/nhess-22-2289-2022

Dixon, L., Izenberg, M., Lempert, R., Patton, A., & Roering, J. (2023). *Residential landslide insurance in Sitka, Alaska: Market conditions and options for improving availability*. RAND Corporation. Retrieved from https://www.rand.org/pubs/perspectives/PEA223-1.html

Fell, R., Ho, K., Lacasse, S., & Leroi, E. (2005). A framework for landslide risk assessment and management. In O. Hungr, R. Fell, R. Couture, & E. Eberhardt (Eds.), *Landslide risk management*. CRC Press.

French, C. (2016). Insuring landslides: America's uninsured natural catastrophes. *Nevada Law Journal*, *17*, 63.

Froude, M., & Petley, D. (2018). Global fatal landslide occurrence from 2004 to 2016. *Natural Hazards and Earth System Sciences*, *18*(8), 2161–2181. https://doi.org/10.5194/nhess-18-2161-2018

Gallen, S., Clark, M., & Godt, J. (2015). Coseismic landslides reveal near-surface rock strength in a high-relief, tectonically active setting. *Geology*, *43*(1), 11–14. https://doi.org/10.1130/G36080.1

Gerstel, W., Brunengo, M., Lingley, W., Logan, R., Shipman, H., & Walsh, T. (1997). Puget Sound bluffs: The where, why, and when of landslides following the Holiday 1996/97 storms. *Washington Geology*, *25*, 17–31.

Godt, J. (2004). *Observed and modeled rainfall conditions for shallow landsliding in the Seattle, Washington, area* (Doctoral dissertation). University of Colorado.

Godt, J., Baum, R., & Chleborad, A. (2006). Rainfall characteristics for shallow landsliding in Seattle, Washington, USA. *Earth Surface Processes and Landforms*, *31*(1), 97–110. https://doi.org/10.1002/esp.1237

Godt, J., Baum, R., Savage, W., Salciarini, D., Schulz, W., & Harp, W. (2008). Transient deterministic shallow landslide modeling: Requirements for susceptibility and hazard assessments in a GIS framework. *Engineering Geology*, *102*(3–4), 214–226. https://doi.org/10.1016/j.enggeo.2008.03.019

Godt, J., Schultz, W., Baum, R., & Savage, W. (2008). Modelling rainfall conditions for shallow landsliding in Seattle, Washington. In R. Baum, J. Godt, & L. Highland (Eds.), *Landslides and engineering geology of the Seattle, Washington area*. The Geological Society of America.

Grant, A. (2017). *Regional-scale coseismic landslide hazard modeling and consequence analysis* (Doctoral dissertation). University of Washington.

Grant, A., Wartman, J., & Abou-Jaoude, G. (2016). Multimodal method for coseismic landslide hazard assessment. *Engineering Geology*, *212*, 146–160. https://doi.org/10.1016/j.enggeo.2016.08.005

Griffiths, D., Huang, J., & deWolfe, G. (2011). Numerical and analytical observations on long and infinite slopes. *International Journal for Numerical and Analytical Methods in Geomechanics*, *35*(5), 569–585. https://doi.org/10.1002/nag.909

Harp, E., Michael, J., & Laprade, W. (2006). *Shallow-landslide hazard map of Seattle, Washington*. USGS Open-File Report 2006-1139. U.S. Geological Survey.

Highland, L. (2003). *An account of preliminary landslide damage and losses resulting from the February 28, 2001, Nisqually, Washington, earthquake*. Open-File Report 03-211. U.S. Geological Survey.

Hungr, O., Clague, J., Morgenstern, N., VanDine, D., & Stadel, D. (2016). A review of landslide risk acceptability practices in various countries. In S. Aversa, L. Cascini, L. Picarelli, & C. Scavia (Eds.), *Landslides and engineered slopes: Experience, theory and practice*. Associazione Geotechnica Italiana.

IPCC. (2022). In H.-O. Pörtner, D. C. Roberts, M. Tignor, E. S. Poloczanska, K. Mintenbeck, A. Alegría, et al. (Eds.), *Climate Change 2022: Impacts, Adaptation, and Vulnerability. Contribution of Working Group II to the Sixth Assessment Report of the Intergovernmental Panel on Climate Change* (p. 3056). Cambridge University Press. https://doi.org/10.1017/9781009325844

Izenberg, M., Clark-Ginsberg, A., Clancy, N., Busch, L., Schmidt, J., & Dixon, L. (2022). Efforts to end a stalemate in landslide insurance availability through inclusive policymaking: A case study in Sitka, Alaska. *International Journal of Disaster Risk Reduction*, *80*, 103202. https://doi.org/10.1016/j.ijdrr.2022.103202

Jeschke, D., Eungard, D., Troost, K., & Wisher, A. (2016). Subsurface database of Washington State—GIS data. Washington Division of Geology and Earth Resources Digital Data Series 11, version 1.2. Retrieved from http://www.dnr.wa.gov/publications/ger_portal_subsurface_database.zip

Jibson, R., & Harp, E. (2016). Ground motions at the outermost limits of seismically triggered landslides. *Bulletin of the Seismological Society of America*, *106*(2), 708–719. https://doi.org/10.1785/0120150141

Khajehzadeh, I., & Vale, B. (2017). How New Zealanders distribute their daily time between home indoors, home outdoors and out of home. *Kōtuitui: New Zealand Journal of Social Sciences Online*, *12*(1), 17–31. https://doi.org/10.1080/1177083X.2016.1187636

King County Department of Assessment. (2020). Assessments data download. Retrieved from https://info.kingcounty.gov/assessor/DataDownload/default.aspx

Lancaster, J., Swanson, B., Lukashov, S., Oakley, N., Lee, J., Spangler, E., et al. (2021). Observations and analyses of the 9 January 2018 debris-flow disaster, Santa Barbara County, California. *Environmental & Engineering Geoscience*, *27*(1), 3–27. https://doi.org/10.2113/EEG-D-20-00015

Lanni, C., Borga, M., Rigon, R., & Tarolli, P. (2012). Modelling shallow landslide susceptibility by means of a subsurface flow path connectivity index and estimates of soil depth spatial distribution. *Hydrology and Earth System Sciences*, *16*(11), 3959–3971. https://doi.org/10.5194/hess-16-3959-2012

Laprade, W. (2007). Effects of urbanization and development on mass wasting. AEG Special Publication No. 22. In A. Turner & R. Schuster (Eds.), *Landslides and Society: Keynote and Invited Presentations at the 1st North American Landslide Conference, Vail, Colorado, June 3–8, 2007*.

Laprade, W., Kirkland, T., Nashem, W., & Robertson, C. (2000). *Seattle landslide study*. Internal Report W-7992-01. Shannon & Wilson Inc.

Laprade, W., & Tubbs, D. (2008). Landslide mapping in Seattle, Washington. In R. Baum, J. Godt, & L. Highland (Eds.), *Landslides and engineering geology of the Seattle, Washington area*. The Geological Society of America.

Larsen, I., Montgomery, D., & Korup, O. (2010). Landslide erosion controlled by hillslope material. *Nature Geoscience*, *3*(4), 247–251. https://doi.org/10.1038/ngeo776

Lee, M., & Jones, D. (2023). *Landslide risk assessment* (3rd ed.). ICE Publishing.

Lempert, R., Busch, L., Brown, R., Patton, A., Turner, S., Schmidt, J., & Young, T. (2023). Community-level, participatory co-design for landslide warning with implications for climate services. *Sustainability*, *15*(5), 4294. https://doi.org/10.3390/su15054294

Maier, S. (1997). In Seattle, lessons have been learned and lessons have been spurned. *The Seattle Post-Intelligencer*.

Medwedeff, W., Clark, M., & Zekkos, D. (2025). Regional back-analysis of earthquake triggered landslide inventories: A 2D method for estimating rock strength from remote sensing data. *Journal of Geophysical Research: Earth Surface*, *130*(1), e2023JF007471. https://doi.org/10.1029/2023JF007471

Microsoft. (2024). GlobalMLBuildingFootprints [Dataset]. *GitHub*. Retrieved from https://github.com/microsoft/GlobalMLBuildingFootprints/

Miller, D. (2016). *Literature synthesis of the effects of forest practices on glacial deep-seated landslides and groundwater recharge*. Report prepared for the Upslope Processes Scientific Advisory Group Cooperative Monitoring, Evaluation, and Research Committee, Personal Services Contract PSC 16-206. M2 Environmental Services. Retrieved from https://www.dnr.wa.gov/publications/bc_tfw_nonglaciallit_20171005.pdf

Mills, A., Francis, T., Shandas, V., Whittaker, K., & Graybill, J. (2008). Using best available science to protect critical areas in Washington state: Challenges and barriers to planners. *Urban Ecosystems*, *12*(2), 157–175. https://doi.org/10.1007/s11252-008-0071-x
Mirus, B., Belair, G., Wood, N., Jones, J., & Martine, S. (2024). Parsimonious high-resolution landslide susceptibility modeling at continental scales. *AGU Advances*, *5*, e2024AV001214. https://doi.org/10.1029/2024AV001214
Miscolta-Cameron, A. (2016). *Science and strategy: How scientific and technical information are used in disputes over landslide regulations in Seattle, WA* (Masters thesis). Western Washington University.
Neiman, P., Schick, L., Ralph, F., Hughes, M., & Wick, G. (2011). Flooding in western Washington: The connection to atmospheric rivers. *Journal of Hydrometeorology*, *12*(6), 1337–1358. https://doi.org/10.1175/2011JHM1358.1
NOAA. (2024). Daily summaries station details: Seattle Tacoma airport, WA US [Dataset]. *National Oceanic and Atmospheric Administration*. Retrieved from https://www.ncdc.noaa.gov/cdo-web/datasets/GHCND/stations/GHCND:USW00024233/detail
Patton, N., Lohse, K., Godsey, S., Crosby, B., & Seyfried, M. (2018). Predicting soil thickness on soil mantled hillslopes. *Nature Communications*, *9*(1), 3329. https://doi.org/10.1038/s41467-018-05743-y
Peck, M., & Payne, D. (2003). Development of an estimated water-table map for coastal Georgia and adjacent parts of Florida and South Carolina. In K. Hatcher (Ed.), *Proceedings of the 2003 Georgia Water Resources Conference*. University of Georgia.
Pesaresi, M., Huadong, G., Blaes, X., Erlich, D., Ferri, S., Gueguen, L., et al. (2013). A global human settlement layer from optical HR/VHR RS data: Concept and first results. *IEEE Journal of Selected Topics in Applied Earth Observations and Remote Sensing*, *6*(5), 2102–2131. https://doi.org/10.1109/JSTARS.2013.2271445
Petley, D. (2025a). Fatal landslides in 2024. *Eos: The Landslide Blog*. https://eos.org/thelandslideblog/fatal-landslides-in-2024
Petley, D. (2025b). Fatal landslides in July 2025. *Eos: The Landslide Blog*. https://eos.org/thelandslideblog/fatal-landslides-in-july-2025
Planet Team. (2020). Planet application program interface: In space for life on Earth. Retrieved from https://www.planet.com/
Pollock, W. (2020). *A framework for regional scale quantitative landslide risk analysis* (Doctoral dissertation). University of Washington. Retrieved from http://hdl.handle.net/1773/45904
Pollock, W., Grant, A., Wartman, J., & Abou-Jaoude, G. (2019). Multimodal method for landslide risk analysis. *MethodsX*, *6*, 827–836. https://doi.org/10.1016/j.mex.2019.04.012
Pollock, W., & Wartman, J. (2020). Human vulnerability to landslides. *GeoHealth*, *4*(10), e2020GH000287. https://doi.org/10.1029/2020GH000287
Pollock, W., & Wartman, J. (2025). MM_3: Multimodal framework for regional-scale quantitative landslide risk analysis. *MethodsX*, *14*, 103218. https://doi.org/10.1016/j.mex.2025.103218
Provant, Z., & Carey, M. (2023). Hazard zone conflicts in the avalanche capital: Stress points for avalanche and landslide mitigation in Juneau, Alaska. *International Journal of Disaster Risk Reduction*, *98*, 104111. https://doi.org/10.1016/j.ijdrr.2023.104111
Quantum. (2016). *PSLC king county delivery 1 LiDAR: Technical data report*. Quantum Spatial.
Rath, J., Roy, S., & Butcher, J. (2017). *Intensity duration frequency curves and trends for the City of Seattle: Technical memorandum*. Report for the Seattle Public Utilities CSO Reduction Program. Tetra Tech.
Reichenbach, P., Rossi, M., Malamud, B., Mihir, M., & Guzzetti, F. (2018). A review of statistically-based landslide susceptibility models. *Earth-Science Reviews*, *180*, 60–91. https://doi.org/10.1016/j.earscirev.2018.03.001
Rose, K. (2021). Sitka Assembly removes landslide section from city code. *KCAW*.
Salciarini, D., Godt, J., Savage, W., Baum, R., & Conversini, P. (2008). Modelling landslide recurrence in Seattle, Washington, USA. *Engineering Geology*, *102*(3–4), 227–237. https://doi.org/10.1016/j.enggeo.2008.03.013
Santi, P., Hewitt, K., VanDine, D., & Cruz, E. (2011). Debris-flow impact, vulnerability, and response. *Natural Hazards*, *56*(1), 371–402. https://doi.org/10.1007/s11069-010-9576-8
Schmidt, K., Roering, J., Stock, J., Deitrich, W., Montgomery, D., & Schaub, T. (2001). The variability of root cohesion as an influence on shallow landslide susceptibility in the Oregon Coast Range. *Canadian Geotechnical Journal*, *38*(5), 995–1024. https://doi.org/10.1139/t01-031
Schulz, W. (2005). *Landslide susceptibility estimated from mapping using light detection and ranging (LIDAR) imagery and historical landslide records, Seattle, Washington*. USGS Open-File Report 2005-1405. U.S. Geological Survey.
Schulz, W., Lidke, D., & Godt, J. (2008). Modeling the spatial distribution of landslide-prone colluvium and shallow groundwater on hillslopes of Seattle, WA. *Earth Surface Processes and Landforms*, *33*(1), 123–141. https://doi.org/10.1002/esp.1535
Seattle Geodata. (2018a). Building Outlines 2015 [Dataset]. *Seattle Geodata*. Retrieved from https://data-seattlecitygis.opendata.arcgis.com/datasets/SeattleCityGIS::building-outline-2015/about
Seattle Geodata. (2018b). ECA potential slide areas [Dataset]. *Seattle Geodata*. Retrieved from https://data-seattlecitygis.opendata.arcgis.com/datasets/SeattleCityGIS::eca-potential-slide-areas-1/about
Seattle Geodata. (2023). ECA known slide events [Dataset]. *Seattle Geodata*. Retrieved from https://data-seattlecitygis.opendata.arcgis.com/datasets/SeattleCityGIS::eca-known-slide-events-1/about
Seattle Office of Emergency Management (OEM). (2019). Seattle hazard identification and vulnerability analysis v7.0. Retrieved from https://www.seattle.gov/emergency-management/hazards
Shipman, H. (2001). *Coastal landsliding on Puget Sound: A review of landslides occurring between 1996 and 1999*. Report #01-06-019. Washington State Department of Ecology. Retrieved from https://fortress.wa.gov/ecy/publications/SummaryPages/0106019.html
Strouth, A., & McDougall, S. (2022). Individual risk evaluation for landslides: Key details. *Landslides*, *19*(4), 977–991. https://doi.org/10.1007/s10346-021-01838-8
Tefsa, T., Tarboton, D., Chandler, D., & McNamara, J. (2009). Modeling soil depth from topographic and land cover attributes. *Water Resources Research*, *45*(10), W10438. https://doi.org/10.1029/2008WR007474
Townsend, K., Gallen, S., & Clark, M. (2020). Quantifying near-surface rock strength on a regional scale from hillslope stability models. *Journal of Geophysical Research: Earth Surface*, *125*(7), e2020JF005665. https://doi.org/10.1029/2020JF005665
Troost, K., & Booth, D. (2008). Geology of Seattle and the Seattle area, Washington. In R. Baum, J. Godt, & L. Highland (Eds.), *Landslides and engineering geology of the Seattle, Washington area*. The Geological Society of America.
Tubbs, D. (1974). *Landslides in Seattle*. Information Circular No. 52. Washington Department of Natural Resources.
UNDRR. (2017). *National disaster risk assessment: Governance system, methodologies, and use of results*. United Nations Office for Disaster Risk Reduction. Retrieved from https://www.unisdr.org/files/52828_nationaldisasterriskassessmentpart1.pdf
UNDRR. (2022). *Global assessment report on disaster risk reduction (GAR2022): Our world at risk: Transforming governance for a resilient future*. United Nations Office for Disaster Risk Reduction. Retrieved from https://www.undrr.org/media/79595/download?startDownload=20251019
U.S. Census Bureau. (2020). Explore census data. Retrieved from https://data.census.gov/cedsci/
USGS. (2018). NSHM: Conterminous U.S. 2018. Retrieved from https://github.com/usgs/nshm-cous-2018

Van Asch, T., Buma, J., & Van Beek, L. (1999). A view on some hydrological triggering systems in landslides. *Geomorphology*, *30*(1–2), 25–32. https://doi.org/10.1016/S0169-555X(99)00042-2

van Westen, C., van Asch, T., & Soeters, R. (2006). Landslide hazard and risk zonation—Why is it still so difficult? *Bulletin of Engineering Geology and the Environment*, *65*(2), 167–184. https://doi.org/10.1007/s10064-005-0023-0

Wait, T. (2001). *Characteristics of deep-seated landslides in Seattle, Washington* (Masters thesis). Colorado School of Mines.

Wartman, J., Montgomery, D., Anderson, S., Keaton, J., Benoit, J., dela Chapelle, J., & Gilbert, R. (2016). The 22 March 2014 Oso landslide, Washington, USA. *Geomorphology*, *253*, 275–288. https://doi.org/10.1016/j.geomorph.2015.10.022

Williams, D. (2015). *Too high & too steep: Reshaping Seattle's topography*. University of Washington Press.

Youngmann, C. (Ed.). (1979). *King county: Coastal zone atlas of Washington*. Washington Department of Ecology.

References From the Supporting Information

Baum, R., Godt, J., & Coe, J. (2011). Assessing susceptibility and timing of shallow landslide and debris flow initiation in the Oregon Coast Range, USA. In R. Genevois, D. Hamilton, & A. Prestininzi (Eds.), *Proceedings of the 5th International Conference on debris Flow Hazards Mitigation—Mechanics, Prediction, and Assessment*.

Biasutti, M., Seager, R., & Kirschbaum, D. (2016). Landslides in West Coast metropolitan areas: The role of extreme weather events. *Weather and Climate Extremes*, *14*, 67–79. https://doi.org/10.1016/j.wace.2016.11.004

Brien, D., & Reid, M. (2007). *Modeling 3-D slope stability of coastal bluffs, using 3-D ground-water flow, southwestern Seattle, Washington*. Scientific Investigations Report 2007-5092. U.S. Geological Survey.

Brien, D., & Reid, M. (2008). Assessing deep-seated landslide susceptibility using 3-D groundwater and slope-stability analyses, southwestern Seattle, Washington. In R. Baum, J. Godt, & L. Highland (Eds.), *Landslides and engineering geology of the Seattle, Washington area*. The Geological Society of America.

Chleborad, A. (2003). *Preliminary evaluation of a precipitation threshold for anticipating the occurrence of landslides in the Seattle, Washington, area*. USGS Open-File Report 03-463. U.S. Geological Survey.

Chleborad, A., Baum, R., & Godt, J. (2006). *Rainfall thresholds for forecasting landslides in the Seattle, Washington, area—Exceedance and probability*. USGS Open-File Report 2006-1064. U.S. Geological Survey.

Daily Star Mirror. (1913). Landslide at Seattle kills one, hurts 3. *The Daily Star-Mirror*.

Debray, S., & Savage, W. (2001). *A preliminary finite-element analysis of a shallow landslide in the Alki area of Seattle, Washington*. USGS Open-File Report 01-0357. U.S. Geological Survey.

Evans, S. (1994). Draining Seattle—WPA landslide stabilization projects, 1935–1941. *Washington Geology*, *22*, 3–10.

Frattini, P., & Crosta, G. (2013). The role of material properties and landscape morphology on landslide size distributions. *Earth and Planetary Science Letters*, *361*, 310–319. https://doi.org/10.1016/j.epsl.2012.10.029

Godt, J., & McKenna, J. (2008). Numerical modeling of rainfall thresholds for shallow landsliding in the Seattle, Washington, area. In R. Baum, J. Godt, & L. Highland (Eds.), *Landslides and engineering geology of the Seattle, Washington area*. The Geological Society of America.

Guzzetti, F. (2000). Landslide fatalities and the evaluation of landslide risk in Italy. *Engineering Geology*, *58*(2), 89–107. https://doi.org/10.1016/S0013-7952(00)00047-8

Hungr, O., Leroueil, S., & Picarelli, L. (2014). The Varnes classification of landslide types, an update. *Landslides*, *11*(2), 167–194. https://doi.org/10.1007/s10346-013-0436-y

Jones, A., Kramer, S., & Arduino, P. (2002). *Estimation of uncertainty in geotechnical properties for performance-based earthquake engineering*. PEER Report 2002/16. Pacific Earthquake Engineering Research Center, University of California, Berkeley.

Liu, C.-N., & Wu, C.-C. (2008). Mapping susceptibility of rainfall-triggered shallow landslides using a probabilistic approach. *Environmental Geology*, *55*(4), 907–915. https://doi.org/10.1007/s00254-007-1042-x

MacDonald, N. (1970). Population growth and change in Seattle and Vancouver, 1880–1960. *Pacific Historical Review*, *39*(3), 297–321. https://doi.org/10.2307/3637654

Malamud, B., Turcotte, D., Guzzetti, F., & Reichenbach, P. (2004). Landslide inventories and their statistical properties. *Earth Surface Processes and Landforms*, *29*(6), 687–711. https://doi.org/10.1002/esp.1064

Miller, R. (1973). *Map showing relative slope stability in part of west-central King County, Washington*. Folio of King County, Washington Map I-852 A. U.S. Department of the Interior, United States Geological Survey.

Montgomery, D., Greenberg, H., Laprade, W., & Nashem, W. (2001). Sliding in Seattle: Test of a model of shallow landsliding potential in an urban environment. In M. Wigmosta & S. Burges (Eds.), *Land use and watersheds: Human influence on hydrology and geomorphology in urban and forest areas*. https://doi.org/10.1029/WS002p0059

Morgan, D., & Jones, J. (1999). *Numerical model analysis of the effects of ground-water withdrawals on discharge to streams and springs in small basins typical of the Puget Sound Lowland, Washington*. USGS Open-File Report 95-470. U.S. Geological Survey.

Morgan, D., & McFarland, W. (1996). *Simulation analysis of the ground-water flow system in the Portland Basin, Oregon and Washington*. USGS Water-Supply Paper 2470-B. U.S. Geological Survey.

Nguyen, L. (2013). Evaluation of the relationship between saturated hydraulic conductivity and grain-size distribution of fluvio-glacial deposits, Puget lowland, Washington. (Masters thesis).

Phoon, K.-K., & Kulhawy, F. (1999). Characterization of geotechnical variability. *Canadian Geotechnical Journal*, *36*(4), 612–624. https://doi.org/10.1139/t99-038

Savage, W., Morrissey, M., & Baum, R. (2000). *Geotechnical properties for landslide-prone Seattle-area glacial deposits*. USGS Open-File Report 00-228. U.S. Geological Survey.

Schulz, W. (2007). Landslide susceptibility revealed by LiDAR imagery and historical records, Seattle, Washington. *Engineering Geology*, *89*(1–2), 67–87. https://doi.org/10.1016/j.enggeo.2006.09.019

Seattle Daily Times. (1908). Man killed when land slides. *The Seattle Daily Times*.

Seattle Daily Times. (1909). Denny Hill regrade claims another victim. *The Seattle Daily Times*.

Seattle Daily Times. (1916a). Gurney funeral to be held tomorrow. *The Seattle Daily Times*.

Seattle Daily Times. (1916b). Six West Seattle homes swept by avalanche. *The Seattle Daily Times*.

Seattle Daily Times. (1942). Daughter tells of fatal slide. *The Seattle Daily Times*.

Seattle Post-Intelligencer. (1899a). County is absolved. *Seattle Post-Intelligencer*.

Seattle Post-Intelligencer. (1899b). Damages for a child's death. *Seattle Post-Intelligencer*.

Seattle Post-Intelligencer. (1914). Family swept in their home down a bluff. *Seattle Post-Intelligencer*.

Seattle Post-Intelligencer. (1922). Two killed in landslide at Endolyne. *The Seattle Post-Intelligencer*.

Seattle Star. (1921). Sluicing for bodies of 3, two more die. *The Seattle Star*.

Shannon & Wilson, Inc. (2003). Seattle landslide study update, addendum to the Seattle landslide study, stability improvement areas. Consultant report 21-1-08913-016 for Seattle Public Utilities.

St. Paul Globe. (1900). *Red wing notes*. The St. Paul Globe.

Tanyas, H., Allstadt, K., & van Westen, C. (2018). An updated method for estimating landslide-event magnitude. *Earth Surface Processes and Landforms*, *43*(9), 1836–1847. https://doi.org/10.1002/esp.4359

Tanyas, H., van Westen, C., Allstadt, K., & Jibson, R. (2019). Factors controlling landslide frequency-area distributions. *Earth Surface Processes and Landforms*, *44*(4), 900–917. https://doi.org/10.1002/esp.4543

The Viet, T., Lee, G., Minh Thu, T., & Uk An, H. (2017). Effect of digital elevation model resolution on shallow landslide modeling using TRIGRS. *Natural Hazards Review*, *18*(2), 04016011. https://doi.org/10.1061/(ASCE)NH.1527-6996.0000233

Thomas, B., Wilkinson, J., & Embrey, S. (1997). *The ground-water system and ground-water quality in Western Snohomish County, Washington*. USGS Water-Resources Investigations Report 96-4312. U.S. Geological Survey.

Tubbs, D. (1975). *Causes, mechanisms and prediction of landsliding in Seattle* (Doctoral dissertation). University of Washington.

USDA. (2019). *ROSETTA class average hydraulic parameters*. U.S. Department of Agriculture, Agriculture Research Service. Retrieved from https://www.ars.usda.gov/pacific-west-area/riverside-ca/agricultural-water-efficiency-and-salinity-research-unit/docs/model/rosetta-class-average-hydraulic-parameters/

Vaccaro, J., Woodward, D., Gannett, M., Jones, M., Collins, C., Caldwell, R., & Hansen, A. (1997). *Summary of the Puget-Willamette Lowland regional aquifer-system analysis, Washington, Oregon, and British Columbia*. USGS Open-File Report 96-353. U.S. Geological Survey.

Van Den Eeckhaut, M., Poesen, J., Govers, G., Verstraeten, G., & Demoulin, A. (2007). Characteristics of the size distribution of recent and historical landslides in a populated hilly region. *Earth and Planetary Science Letters*, *256*(3–4), 588–603. https://doi.org/10.1016/j.epsl.2007.01.040

Wang, Y. (2014). *Probabilistic assessments of the seismic stability of slopes: Improvements to site-specific and regional analyses*. (Doctoral dissertation). University of Texas at Austin.

Wang, Y., & Rathje, E. (2015). Probabilistic seismic landslide hazard maps including epistemic uncertainty. *Engineering Geology*, *196*, 313–324. https://doi.org/10.1016/j.enggeo.2015.08.001

Washington Forest Practices Board (WFPB). (2016). Guidelines for evaluating potentially unstable slopes and landforms. Washington Forest Practices Board Manual, Section 16.2. Retrieved from https://www.dnr.wa.gov/about/boards-and-councils/forest-practices-board/rules-and-guidelines/forest-practices-board-manual

Welsch, W., Frans, L., & Olsen, T. (2014). *Hydrogeologic framework, groundwater movement, and water budget of the Kitsap Peninsula, west-central Washington*. USGS Scientific Investigations Report 2014-5106. U.S. Geological Survey.